In: Simulation of Membrane Reactors
Editor: Angelo Basile and Fausto Gallucci
ISBN: 978-1-60692-425-9

Chapter 6

POLYMERIC MEMBRANE REACTORS

José M. Sousa[1,2], Luís M. Madeira[2], João C. Santos[2] and Adélio Mendes[2]

ABSTRACT

The aim of this chapter is the study of membrane reactors with polymeric membranes, particularly catalytic polymeric membranes. After an introduction where the main advantages and disadvantages of the use of polymeric membranes are summarised, a review of the main areas where they have been applied, integrated in chemical reactors, is presented. This excludes the field of bio-membranes processes, which is analysed in a specific chapter of this book. Particular attention is then given to modelling works in the fields of polymeric catalytic membrane reactors, where the membrane is catalytic itself. The various models that have been presented in the literature, as well as the numerical details regarding the respective mathematical equations, are shown and discussed. At the end, 3 different examples are presented and solved with the software package "MADONNA".

INTRODUCTION

To some extent, a membrane reactor (MR) is a device where a combination of a membrane and a chemical reactor must integrally couple in such a way that a synergy is created between the two systems. Particularly interesting is the possibility of overcoming equilibrium in reversible reactions, where MRs is one technology, among several others, to accomplish that. Improved selectivity is also of concern, as described below. A more comprehensive introduction on membrane reactors is present in chapter 1 of this book.

[1] Chemistry Department, University of Trás-os-Montes e Alto Douro, Vila-Real, Portugal
[2] LEPAE – Department of Chemical Engineering, Faculty of Engineering – University of Porto, Porto, Portugal

ADVANTAGES AND LIMITATIONS OF THE POLYMERIC MEMBRANE REACTORS

In addition to the general advantages of combining reaction and membranes, the use of polymeric catalytic membranes in MRs can lead to some new important possibilities, as recently reviewed by Ozdemir *et al.* [1]. For instance, when a heterogeneous catalyst (nanosized metal cluster, zeolite or activated carbon, for example) is incorporated into a polymeric matrix, the selective sorption of reagents and products can be adjusted with a well-chosen polymeric environment, which may result in a potential beneficial effect on the catalytic performance. On the other hand, a much wider choice of polymeric membranes is available to select the most appropriate for membrane-assisted processes, as compared with metallic or ceramic membranes. Moreover, the technology to manufacture polymeric membranes is generally better developed. For these reasons, polymeric membranes have found a wide range of industrial applications in gas separation, and in some cases such processes have become a standard [2]. However, their use associated with reactors, particularly in the biotechnology field, is also of concern [1, 3].

Because polymeric membranes are less resistant to high temperatures, aggressive solvents/chemicals and oxidative conditions than their inorganic or metallic counterparts, polymeric membrane reactors (PMRs) may only be used in processes conducted at mild conditions. But yet, these limitations are relative: Nafion® and polydimethylsiloxane (PDMS), the two most widely used polymers to make catalytic polymeric membranes [4, 5], proved already to remain stable even under rather harsh conditions, showing an excellent thermal, mechanical and chemical resistance [5]. Moreover, the recent development of thermally resistant polymeric membranes [6, 7] provides promise for the more widespread use of such materials in MRs applications. On the other hand, polymeric membranes show some important advantages over the inorganic counterparts in their potential use as catalytic devices: their thickness can be controlled easily, a large scale preparation is not difficult, they are easier to be prepared crack-free and in different shapes (hollow, spiral wound, flat sheet, etc.), they are cheaper [1, 8] and they show versatile diffusivities and sorption capacities [9]. Besides, they may exhibit higher selectivities. Conversely, membrane permeability is often limiting.

Another potential interesting feature of the polymeric catalytic membranes is that they may actively take part in the reaction by different ways. Firstly, the influence on the sorption capacity of reagents and products must be considered, because the concentration of the reaction species near the active sites depends directly on the sorption capacity. This sorption capacity depends strongly on the degree of polymer cross-linking, which is determined, in first instance, by the polymer composition, but the presence of a solid phase catalyst incorporated into the polymer may cause additional physical or even chemical cross-linking [10]. Secondly, the diffusivity of reagents and products is a very important parameter to have also into account, because it is influenced by the global sorption capacity: a high sorption of a component means a strong swelling of the polymer and thus an increased mobility of the diffusing species.

In general, almost only elastomeric polymers are utilized to incorporate homogeneous or heterogeneous catalysts. In fact, as the chains of glassy polymers are much less flexible, the incorporation of fillers disturbs its packing and leads to the occurrence of stresses, which may result in cracks. PDMS has been the most utilized polymer for making polymeric catalytic membranes, because it is cheap, chemically resistant, mechanically and thermally stable (up to 250 °C), easy to prepare and its flexible siloxane chains allow a fast mass transfer through the membrane. This mass transfer resistance could be important in the case of the diffusional controlled regime.

APPLICATION FIELDS OF THE POLYMERIC MEMBRANE REACTORS

In the following, some examples of chemical reactions that have been studied in PMRs, and particularly in polymeric catalytic membrane reactors (PCMRs), will be described, grouped according to the type of reaction. Such analysis excludes the applications in bio-reactors, which have a specific chapter in this book devoted to its analysis (chapter 8), and also in fuel cells, a topic which has deserved the special attention of many reviews and textbooks.

DEHYDROGENATION REACTIONS

Dehydrogenations are endothermic and equilibrium-limited reactions, which should be performed at relatively high temperatures to proceed at reasonable rates and to shift the conversion to levels of practical significance. For such reasons, polymeric membrane reactors have been hardly ever used for conducting these reactions. Among the several tens of references on this subject, which are extensively discussed through this book in the chapter devoted to the inorganic membranes, only Frisch *et al.* [11] reported a study on dehydrogenation reactions conducted in PCMRs. These authors studied the dehydrogenation of cyclohexane to benzene using catalytic polymeric membranes based on polyethylacrylate and a 13X zeolite, which contained a dehydrogenation catalyst (Ti or Ni based). These catalytic membranes showed to be active for the reaction studied at temperatures as low as 50-90 ºC. Rezac *et al.* [12] also described a membrane-assisted dehydrogenation of *n*-butane, consisting of two plug flow reactors in series with an interstage hydrogen-removal polyimide-ceramic composite membrane. However, this is not a typical PCMR.

HYDROGENATION REACTIONS

Hydrogenation reactions conducted in MRs have been studied for long time, e.g. Gryaznov *et al.* [13]. In the early times, palladium membranes were utilized. However, PMRs and in particular PCMRs have also been considerably used for conducting such reactions in the most varied situations, namely gas, liquid and gas/liquid phases.

Partial hydrogenation of multiple-unsaturated hydrocarbons is an important process in the petrochemical industry, used for both purification of alkene feed streams and production of

commodity chemicals from alkynes, dienes and aromatics. In choosing a catalyst for a partial hydrogenation process, selectivity for the intermediate product (e.g. alkene) is more important than catalytic activity. Thus, processes are often run at low temperatures and low hydrogen partial pressures, making promising the use of catalytic polymeric membranes. Table 1 summarises some of the works that have been carried out in this field using such membranes.

Table 1. Some examples of hydrogenation reactions using catalytic polymeric membranes

Main reagent(s)	Catalyst(s)	Membrane/ Support *	Reacting Phases	Operation mode and conditions	Ref.
Cyclopentadiene and isoprene	Pd, Co, Cu, Ni	PPO and PSF	Liquid/gas	Batch reactor, 40 ºC	[14]
Cyclopentadiene, isoprene and butadiene	Pd	PVP, EC and AR	Gas	Membrane contactor, 40 ºC, 0.1 MPa	[15]
1-Octene	Pd	PES-C	Liquid/gas	Batch reactor, 40 ºC	[16]
Propadiene and propyne	Pd	PVP	Gas	Membrane contactor, 40 ºC	[17]
Butadiene	Pd, Pd-Co	PVP, EC and AR	Gas	Membrane contactor, 40 ºC	[18]
Cyclopentadiene	Pd, Pd-Co	PVP, EC and AR	Gas	Membrane contactor, 40 ºC	[19]
Ethylene, propylene and 1,3-butadiene	Pd	diblock copolymers (polyMTD)	Gas	Batch reactor, room temperature/120 °C	[20, 21]
Propylene	Pd	PDMS	Gas	Membrane contactor, 30 ºC	[22]
Propylene and propyne	Pd	PAI	Gas	Membrane contactor, 30 ºC	[23]
Propylene and propyne	Pd	PDMS	Gas	Membrane contactor, 30 ºC	[24, 25]
1,5-Cyclooctadiene, 1-octyne, phenyl acetylene and geraniol	Pd	PAA	Liquid/gas	Pore-through-flow CMR, 323 K, 40 bar H_2 pressure	[26]
Sunflower oil	Pd or Pt	PES and PAI	Gas/liquid	Flow-through contactor, 100 ºC, 4 bar H_2	[27]
Sunflower oil	Pd	Nylon-6	Gas/liquid	Flow-through reactor	[28]
Methylenecyclohexane	Pd	PVDF	Gas/liquid	Total flow-through reactor, 25-50 ºC	[29]
Cyclohexene	Pt	Nafion® and Tosflex®	Gas/liquid	Batch reactor	[30]
4-Chlorophenol	Pd/Rh	PEBA	Liquid	Catalytic pervaporation (PV) reactor; ~25-60 ºC	[31, 32]
Acetophenone	Pd	PDMS and PEBA	Gas/liquid	Catalytic PV reactor; 30-70 ºC, 1-4 bar H_2	[33]

* PPO – poly(phenylene oxide); PSF – polysulfone; PVP – polyvinylpyrrolidone; EC – ethyl-cellulose; AR – melamine-formaldehyde; PES-C – phenophtalein polyethersulfone; MTD – methyltetracyclododecene; PDMS – polydimethylsiloxane; PAI – polyamideimide; PAA – polyacrylic acid; PES – polyethersulfone; PVDF – polyvinylidene fluoride; PEBA – poly(ether-*b*-amide);

Gao and co-workers [14], for example, prepared several metal-containing polymeric materials by incorporating transition metal chlorides (Pd, Co, Cu, Ni) into modified or unmodified poly(phenylene oxide) and polysulfone (cf. Table 1). The catalytic activities and selectivities of these materials were investigated, under mild conditions (40 °C), for the hydrogenation of cyclopentadiene in a liquid/gas phase batch reactor using ethanol as solvent and for the hydrogenation of cyclopentadiene and isoprene in a gas phase batch reactor. In these studies, the membrane acted only as a support of the catalyst. The authors found that both the activity and selectivity of the catalysts in the hydrogenation of cyclopentadiene in the gas phase were lower than those in liquid phase. The reason for the higher activity in liquid phase could be ascribed to the much higher concentration of cyclopentadiene. For the higher selectivity, the very low solubility of hydrogen in ethanol could be pointed out as a reason, which, associated with the higher concentration of cyclopentadiene, inhibited the further hydrogenation of the monoene.

The same group [15] has also studied the selective hydrogenation of cyclopentadiene, isoprene and butadiene in CMRs made of a polymer-anchored palladium catalyst. They used different polymers (cf. Table 1) to anchor the Pd catalyst, which was deposited on the inner wall of hollow fibres. The authors found that all the MRs were active for the selective hydrogenations, though with a strongly dependent efficiency on both the hollow fibre support (cellulose acetate, polysulfone or polyacrylonitrile) and the polymer anchored palladium complex. Besides, they concluded also that the segregated feed of reactants (hydrogen fed to the shell side of the hollow fibre, cyclopentadiene fed to the bore side) was better than the premixed feed (fed to the bore side). As in the previous study [14], the selectivity showed to be strongly dependent on the hydrogen concentration at the reaction site. Slowly feeding hydrogen along the reactor length improves the selectivity by keeping its partial pressure low throughout the reactor, allowing to achieve values as high as 93.4% at a cyclopentadiene conversion of 99.0% [15].

Yu *et al.* [16], on its turn, studied the hydrogenation of 1-octene using a high temperature withstanding polymer, the phenophtalein polyethersulfone. This Pd-containing polymeric material exhibited a large activity for this reaction, as well as the membranes made from this material showed a relatively high permeability. Based on their results, the authors stated that such material may be promising to build a catalytic polymeric membrane reactor for gas phase hydrogenation and dehydrogenation at relatively high temperatures.

Liu *et al.* [17] have also prepared catalytic membranes of poly(N-vinyl-2-pyrrolidone) (PVP)-Pd/cellulose acetate alike the ones referred above [15] for the selective hydrogenation of propadiene and propyne to propene (cf. Table 1). The content of propadiene and propyne reduced from 1.2% and 1.3% to less than 10 and 5 ppm, respectively (the requisites for propene use in polypropylene production), and a high selectivity in the conversion of such components to propene (97.8%) showed that this MR was very effective to conduct these reactions, provided the appropriated hollow fibres and operation conditions had been chosen. The same group has also studied other dehydrogenation reactions, as mentioned in Table 1. For instance, it is worth noting the selective hydrogenation of butadiene to 1-butene [18], where a content of butadiene less than 10 ppm and a maximum 1-butene loss of about 2% could be achieved, while simultaneously inhibiting 1-butene isomerization to 2-butene. Another example is the selective conversion of cyclopentadiene into cyclopentene [19]. In this case, and to further improve the catalytic performance, the reaction was carried out in the bimetallic (Pd-Co) polymeric hollow fibre reactors, with conversion of cyclopentadiene and

selectivity to cyclopentene attaining values as high as 97.5% and 98.4%, respectively. Besides, the activity of the catalytic hollow fibres kept stable during the selective hydrogenations [19], indicating that the polymer-anchored catalysts were firmly retained in the microporous structure of the fibres.

Some groups have used catalytic polymeric membranes with incorporated metallic nanoclusters, an arrangement that offers the possibility to combine the catalytic activity (higher surface area per unit of catalyst volume) with the capacity to selectively remove components from the reaction medium. With this in mind, Ciebien *et al.* [20, 21] prepared catalytic polymeric films by synthesizing palladium nanoclusters within diblock copolymers, with a palladium content of 14 wt. %. These materials showed to be active catalysts for the hydrogenation of ethylene and propylene [20] and 1,3-butadiene [21], even though the clusters were completely surrounded by a bulk polymer matrix. The polymer was able to stabilize the clusters against gross aggregation, but could no prevent some systematic increase in clusters size [20, 21]. The authors found that the hydrogenations were a complex function of the sorption and diffusion coefficients of the reactants in the polymeric matrix, sorption of reactants on the palladium clusters surface, molecular size of reactants, size of clusters, temperature, etc. In another group, Theis *et al*. [22] studied the catalytic activity of a polydimethylsiloxane (PDMS) membrane loaded with palladium nanoclusters (0-15 wt. % metal content), selecting the hydrogenation of propene to propane as test reaction (cf. Table 1). Later on, they studied the same reaction in a polyamideimide ultrafiltration membrane loaded with palladium nanoclusters [23]. The membrane surface was impregnated with an inorganic titanium dioxide layer (up to 40 wt. %), further activated by finely dispersed nanosized palladium clusters. In this way, the palladium catalyst was decoupled from the polymeric surface. For the most active membranes, high conversion of the alkene (up to 100%) and high flux were achieved. In the selective hydrogenation of a stream containing 5% of propyne in propene using the same membranes, a selectivity of 99% to propene at a propyne conversion of 100% was achieved. Besides, these membranes proved to be stable up to temperatures of 200 °C and for operation times up to 50 h.

More recently, these hydrogenations were studied using PDMS-incorporated nanosized Pd, aiming the development and evaluation of mathematical modelling of catalytic membrane reactors [24, 25] as it will be discussed at the end of section "*Modelling of Polymeric Catalytic Membrane Reactors*". The main goal of this hydrogenation was the selective hydrogenation of propyne into propylene, avoiding the subsequent conversion into the alkane.

Table 1 summarizes other relevant works in this field, some of them consisting of reactions conducted in three-phase reactors (gas/liquid/solid-catalyst), where mass transfer limitations often constitute a serious problem in achieving high activities and selectivities and that can be partially overcome with the use of CMRs [28-29]. One field that deserves special attention is the edible oil hydrogenation, particularly selective conversion of sunflower oil [27, 28], in which trans-isomerization is avoided and the expensive noble metal catalysts employed are easily recovered by using MRs. Finally, one should mention the works by Bengtson *et al.* [31-33], who studied the simultaneous enrichment of organic compounds by pervaporation and the concerning reaction within the same catalytic membrane reactor. Firstly, they used poly(ether-*b*-amide) (PEBA) membranes, an elastomer known to effectively concentrate slightly polar chemicals from water [31]. Due to the low affinity of chlorophenol towards palladium and also the very low volume fraction of catalyst (~1% v/v), a considerable amount of this reactant crosses the membrane without meeting any reaction site.

In an attempt to reduce such losses, the experiments were repeated with a catalytic membrane filled with nano-sized silica particles [32]. This membrane showed to be much more active than the one previously used [31], as a result of the considerably lower cluster size and the elongation of the diffusion path through the membrane, increasing thus the contact rates with the catalyst. More recently, acetophenone hydrogenation was studied by a pervaporative catalytic membrane reactor coupled to a mass spectrometer [33], cf. Table 1.

WATER AND WASTEWATER TREATMENT

Although the use of polymeric membrane reactors for water treatment (through hydrogenation processes) could be included in the previous section, we consider that this application is sufficiently relevant to be discussed separately. In this concern, one should first mention the elimination of nitrates from drinking water, a serious problem in many agricultural areas in Europe and in the US. Indeed, limits for nitrate concentrations in drinking water have been imposed, because it has been linked to a number of health hazards. Conventional techniques for nitrates removal (e.g. chemical precipitation of complex salts, distillation, reverse osmosis, electrodialysis, ion exchange and biological treatment) have a number of disadvantages; the physicochemical processes create a waste of highly concentrated brines that must be disposed-off, whilst the biological treatment requires the use of a co-metabolite that, for drinking water applications, also raises other safety concerns. An alternative procedure involving the hydrogenation of nitrates to N_2 in a CMR has been proposed recently, offering several advantages over the established technologies for denitrification. Beyond the CMRs based on inorganic membranes which can be found in many studies, also polymeric membranes have been considered for conducting such processes, as shown in Table 2.

Table 2. Some examples of water and wastewater treatment applications using catalytic polymeric membranes

Pollutant	Catalyst(s)	Membrane/Support *	Phases	Operation mode and conditions	Ref.
Nitrates	Pd-Cu	PEI	Liquid/gas	Membrane contactor	[34]
Nitrates	Pd-Cu	PA	Liquid/gas	Membrane contactor, 25 ºC	[35]
Chlorobenzene	Pd	PDMS/PAN	Liquid/gas	Membrane contactor, 25 ºC	[36]
Chloroaliphatics	TiO_2	PHOTOPERM™	Liquid/gas	Batch mode with total recycling in a flow-through configuration, pilot -scale**	[37, 38]
Phenol	TiO_2	PHOTOPERM™	Liquid	idem	[39]
Chlorophenols	TiO_2	PHOTOPERM™	Liquid	idem	[40]
n-Alkanoic acids	TiO_2	PHOTOPERM™	Liquid/gas	idem but at lab-scale	[41]
Ethylene glycol	TiO_2	microporous PTFE		Batch mode with total recycling in a flow-through configuration	[42]
Several	TiO_2	Several nanofiltration	Liquid/gas	Batch photoreactor and	[43]

pharmaceuticals		membranes (NTR 7410, PAN GKSS HV3/T, N30 F, NF PES 10)		photocatalytic MR and with total recirculation	
Azo dye Orange II	Fe^{3+}	Nafion®	Liquid	Batch photoreactor with recycling	[44]
Phenol	$H_3PW_{12}O_{40}$ (W12)	PVDF	Liquid/gas	Continuous flat-sheet MR with recirculation, 30 ºC	[45]

* PEI – polyetherimide; PA – polyamide; PDMS – polydimethylsiloxane; PAN – poly(acrylonitrile); PTFE – polytetrafluoroethylene; PVDF – polyvinylidene fluoride;
** Membrane module PHOTOPERM® CPP/313 in a coaxial configuration.

Very briefly, Lüdtke *et al.* [34] studied the reduction of nitrate using catalytic microporous polyetherimide membranes. The catalyst incorporated into the membrane matrix consisted of bimetallic microsized clusters containing 4.45 wt. % of palladium and 0.95 wt. % of copper coated on aluminium oxide. Hydrogen (pressure slightly above atmospheric) was permeating from the outer side of the hollow fibre membrane into the nitrate-containing water flowing in the bore side. It was found that the activity decreased by increasing the pH of the solution and increased with the temperature of the solution, though the selectivity to the final product N_2 remained constant in both cases. The authors concluded that the formation of ammonia could be minimized by reducing the catalyst contact time. The reaction within the membrane matrix was dominated by mass transfer.

Later on, Ilinitch *et al.* [35] studied the same reduction reaction using catalytic macroporous polyamide membranes (Table 2). The main goal of the authors was to explain why the coupling of the palladium and copper catalysts in the same membrane gave rise to a multifold increase in the catalytic activity of the aqueous nitrate reduction by hydrogen, comparatively to the values obtained with similar membranes impregnated with each of the catalysts alone. They concluded that it was most likely the hydrogen spillover the main responsible for such behaviour, which consisted in providing reducing agent (hydrogen species) for the reductive regeneration of copper sites.

Beyond nitrates, ground water has been also contaminated with halogenated hydrocarbons, mainly in some industrial areas, despite their low solubility. To study the possibility of treatment of such waters in CMRs, Fritsch *et al.* [36] selected the hydrodechlorination of chlorobenzene as a representative test reaction; the halogen-free hydrocarbons are then more readily degraded by microorganisms in subsequent biological treatment units. The experiments were conducted in a three-phase CMR operating in interfacial contact mode (cf. Table 2). With such an arrangement, the supplying of hydrogen from the gas phase to the catalyst through the PDMS membrane is decoupled from its limited solubility in water. PDMS is a hydrophobic elastomer that, besides preventing direct access of all potential contaminants in the aqueous phase (e.g. heavy metals or some sulphur compounds) to the catalyst (allowing nevertheless that organic reactants cross it), shows a high permeability towards hydrogen. Though the catalytic activity attained in the MR proved to be enough for the purpose of the target application, the authors found a continuous decrease of activity, suspecting that this might be due to a possible partial poisoning of the catalyst by adsorbed chlorine.

Apart from water treatment, wastewater management is nowadays another issue of concern because conventional methods are often not convenient (e.g. incineration for diluted aqueous wastes or biodegradation for toxic compounds). Therefore, attention has recently

been given to alternative and innovative technologies for elimination or detoxification of hazardous organic wastes, frequently referred to as advanced oxidation processes (AOPs). Briefly, the AOPs generally include the addition of oxidizing agents (hydrogen peroxide, ozone, or molecular oxygen itself) in the presence of a catalyst, ultraviolet radiation (UV) or both, therefore providing the formation of highly oxidative radicals, like the hydroxyl ones. Among several others AOPs, the photocatalytic processes are an important class, which has been proposed as a viable alternative for the decontamination of either wastewater or drinking water for human use, namely for the degradation of different toxic organic compounds – particularly chlorinated ones. In these processes, the activation of a finely divided semiconductor by UV radiation, usually titanium dioxide, in intimate contact with an aqueous solution of the pollutants, develops a redox environment capable of oxidizing them into non-toxic substances. Slurry-type reactors making use of TiO_2 suspensions seem to be more efficient than those based on immobilized catalyst, but, for engineering applications, they suffer from an intrinsic drawback: the need of a post-treatment for catalyst recycling and for the ultimate goal of obtaining clean and powder-free water [46]. For this reason, anchoring the TiO_2 to a suitable support or impregnating it in a polymer is desirable. In this last case, a UV transparent membrane matrix with a good adsorption capacity for the organic compounds is required.

With these goals in mind, many studies have been carried out focusing in the degradation of several compounds in potable waters and wastewater, being of particular relevance those of Bellobono and co-workers, a few of which are summarised in Table 2. Outstanding results obtained by the photocatalytic membrane technology used in these works, patented by Chimia Prodotti e Processi, Milan, Italy [47] and developed up to pre-industrial scale, have showed that these membranes are very useful and promising for degrading several compounds. Comparing with the suspended semiconductor reactors, the CMRs (even without promoting photocatalysts) showed more than twofold gain in rate [37]. Besides photomineralization, the PHOTOPERM® process showed also to be suitable for the pre-treatment of wastewater containing a broad variety of non-biodegradable contaminants, specifically toxic compounds, preceding a biological treatment [37].

Ingested pharmaceuticals, used for medical and veterinary purposes, are usually present in wastewaters, because they are not completely metabolized. Because they are often difficult to (bio)degrade or remove using conventional treatments, they appear in the effluents in concentrations of up to several mg/L. This way, the photooxidation of different pharmaceuticals with oxygen by using a hybrid photocatalytic MR was performed recently [43], cf. Table 2, but further investigation seems to be still in progress. In particular, the membrane rejection towards the pollutants was not very satisfactory.

Another interesting example is the use of the photo-Fenton process to abate a non-biodegradable azo dye (Orange II) using a CMR, as described by Lopez and Kiwi [44]. In their work, the authors impregnated a Nafion® membrane with Fe^{3+} ions through a ion-exchange process. The membrane was floating freely in the solution and was used to eliminate the need of removal of the free iron ions in wastewater after pollutant degradation, as occurs in a homogeneous process. The degradation was based on the enhanced generation of mainly OH radicals from H_2O_2 in the presence of the Fe^{3+} species by UV radiation. Finally, it was reported recently a study in which another photocatalyst has been used – Keggin type phosphotungstic acid, $H_3PW_{12}O_{40}$ (W12) –, one of the most widely used photocatalytic

polyoxometalates, which was supported on the surface of plasma-activated PVDF membranes [45] (cf. Table 2).

OXIDATION/EPOXIDATION REACTIONS

Oxidation reactions in the fine chemical synthesis frequently involve immiscible reactants, namely organic and aqueous (mainly peroxide) phases. Due to this immiscibility, which leads to a much lower concentration of the organic reactant in the aqueous phase and vice-versa, the reaction rates are quite low in a conventional batch reactor, where the catalyst particles are suspended. Usually, a co-solvent or phase transfer agents must be added to increase the mutual solubilities, thus increasing the reaction rates. However, phase transfer agents are not of generalized applicability, and the addition of a solvent inevitably decreases reagent concentrations. Moreover, both ways often complicate the separation of the products from the reaction mixture afterwards.

One way to circumvent these problems is using a MR with catalytically active species incorporated into polymeric membranes. In general, such reactions are conducted at mild conditions, perfectly suitable for the limited chemical and thermal resistance of these materials. However, there are many other advantages associated with the use of PCMRs in such applications: i) the influence of the polymer surrounding the catalyst creates the possibility of fine-tuning the sorption of reactive species in the catalyst by choosing the appropriate polymer material; ii) a dense membrane can be used to keep the two reagent phases separated, eliminating the need of a solvent in the case of immiscible reactants (more environmentally-friendly system); iii) the easy separation of the solid catalyst from the reaction mixture; and iv) the facilitated subsequent product purification.

The mostly used polymer for these reactions has been the PDMS. As the aqueous peroxide solutions have to react with nonpolar hydrocarbons, a hydrophobic polymeric membrane is preferred, acting as a reservoir for nonpolar compounds and, simultaneously, excluding excessive amounts of polar substances from the active sites. This is very important to minimize peroxide decomposition. Especially in the case of substrates with low reactivity, where the oxidant strongly competes for reaction, it is crucial to properly adjust the organic substrate/oxidant ratio at the active site. On the other hand, incorporation of catalysts into the membrane provides not only increases in selectivity and/or activity, but the polymeric matrix results in a rather easy way of good dispersion of the catalysts, which might therefore be more easily recycled, being this issue particularly interesting for the more expensive catalysts like the chiral transition metal complexes.

Table 3 gives an overview about important examples of catalytic polymeric membranes applications in oxidation processes. The first one, by Parton *et al.* [48], concerns possibly the former study in which a solid catalyst was dispersed in a dense organic polymer to create a room temperature (RT) catalytic polymeric membrane. The authors occluded the zeozyme FePcY (iron-phthalocyanine complex encapsulated in the cages of a zeolite Y, a mimic of the enzyme cytochrome P-450 that controls the rate of radicals formation in the nature) in a PDMS polymer for the cyclohexane oxidation with *t*-butylhydroperoxide. A remarkable 6-fold increase in activity was observed, as compared with the best possible experimental setup for non-embedded FePcY, a fed-batch liquid phase reactor (where the addition of peroxide to

the reaction mixture was controlled, in order to lower its concentration in the zeolite and to balance it with the alkane one). Such increased activity was caused by the different properties of sorption and diffusion of the reactants and products into PDMS polymer. The cyclohexane (and *n*-dodecane) oxidation was investigated further by the same group [49-51] using also a liquid phase CMR. In particular, they found that such CMR could actually be applied to integrate reaction and a full separation in one single process unit, since the reaction products were exclusively recovered from the organic phase, particularly in the case of *n*-dodecane oxidation (because dodecanol and dodecanone products are not soluble in water) [49].

Table 3. Some examples of oxidation/epoxidation reactions using catalytic polymeric membranes

Main reagent(s)	Catalyst(s)	Membrane/ Support *	Phases	Operation mode and conditions	Ref.
Cyclohexane and *n*-dodecane	Zeozyme FePcY	PDMS	Liquid	Batch and interfacial contact, RT	[48-51]
Cyclohexene and styrene	Zeozyme $[Mn(bpy)_2]^{2+}$–NaY zeolite	PDMS	Liquid	Batch and fed-batch reactors, RT	[52]
Hydroxyl alkene 3-penten-2-ol	Mn-porphyrin complexes	PDMS	Liquid	Batch reactor, RT	[53]
Cyclic alcohols	Mn- and Fe- porphyrin complexes	PDMS	Liquid	Batch reactor, RT	[54]
n-hexane	Microporous Ti silicalite zeolite	PDMS	Liquid/ Gas	Interfacial contact	[55, 56]
Propylene (and other organics)	Microporous Ti silicalite zeolite	PDMS	Liquid/ Gas	Interfacial contact	[57]
2-Propanol and etanol	$H_3PMo_{12}O_{40}$ and $H_5PMo_{10}V_2O_{40}$	PSF, PES and PPO	Gas	Flow-through reactor, 120-210 ºC	[58, 59]
Light alkanes (methane, etane and propane)	Superacid catalysts and Fenton system	Nafion-based and others	Liquid/ Gas	Interfacial contact, 70-120 ºC, 140 kPa	[60-66]
Sulphides	Sodium salt of tetra(sulfophthalocyanine) Co (II))	PA/PVA thin film composite RO/NF membranes	Liquid	Batch and flow-through reactors, RT	[67]
1-Butanol and 1-hexanol	Complexes of Cu- and Co-tetraphenylporphyrinate	Cation exchange perfluorated membranes	Liquid/ Gas	Interfacial contact, 60-70 ºC	[68]
Secondary amines	Sodium tungstate (Na_2WO_4)	PVDF	Liquid	Flat MR, recirculation mode, 25 ºC	[69]
Benzene	Fe and Cu salts	PP, PAN and PTFE	Liquid/ Liquid	Batch reactor with two phases, 35 ºC	[70]

* PDMS – polydimethylsiloxane; PSF – polysulfone; PES – polyethersulfone; PPO – polyphenylene oxide; PA – polyamide; PVA – poly (vinyl alcohol); RO – reverse osmosis; NF – nanofiltration; PVDF – poly(vinyldene difluoride); PP – polypropylene; PAN – polyacrylonitrile; PTFE – polytetrafluoroethylene;

A specific and important problem occurring in liquid phase reactions with homogeneous catalysts occluded into membranes is the leaching of the complex and/or of the co-

incorporated additive out of the membrane. For that reason, several studies have been reported addressing this issue, e.g. Neys *et al*. [53], and proposing strategies to reduce leaching, namely establishing a chemical bond between the complex and the polymer [5], placing bulky groups on the catalyst [5] or selecting more appropriate reaction conditions (for instance, by using solvents that combine moderate swelling with low solubility of the complex) [5, 50]. Modifying the polymeric matrix may also restrict leaching.

Other relevant works regarding oxidation reactions are summarised in Table 3, although many others can be found in the scientific literature. One example mentioned therein is the oxyfunctionalization of *n*-hexane with hydrogen peroxide into a mixture of hexanols and hexanones, performed by Kaliaguine and co-workers [55, 56], a work that is discussed more deeply in the section "*Liquid/Vapour Phase Membrane Reactors*". This group also patented a gas-liquid or liquid-liquid catalytic polymeric membrane interphase contactor, reporting the epoxidation of propylene and the oxygenation of organic compounds such as *n*-hexane with dilute (30 wt. %) aqueous hydrogen peroxide solution [57]. The system consisted of a zeolite (titanium silicalite, TS-1) occluded into a polymeric matrix of pure or silane-modified PDMS (cf. Table 3). In the case of the propylene epoxidation, the secondary reactions could be suppressed because, as opposed to the bubble-slurry reactor, the dissolved propylene and propylene oxide do not remain in permanent contact with the hydrogen peroxide solution and the TS-1 catalyst. Actually, with the MR the propylene oxide is dissolved in the H_2O_2 solution, no longer contacting the catalyst.

Another interesting study is that reported by Lee and co-workers, who combined different types of heteropolyacids (HPAs) with a set of polymers [58, 59]. When a mixture of 2-propanol and air was permeated through the catalytic membrane, two competitive parallel reactions took place: an acid catalyzed dehydration to propylene and an oxidative dehydrogenation to acetone via a redox mechanism [58]. Compared with a reaction in a fixed bed, the incorporation of the HPMo ($H_3PMo_{12}O_{40}$) catalyst in the membrane drastically changed the reaction selectivity. Firstly, the dimethylformamide used as casting solvent sorbed strongly on the acidic sites of the HPMo, thus greatly decreasing the acid catalyzed reaction (propylene formation). Secondly, the incorporated catalyst was much more active in the oxidative dehydrogenation (formation of acetone) due to the enlarged active surface, which was created by the uniform and fine distribution of the HPMo in the polysulfone membrane. Thirdly, the higher permeability of the membrane towards acetone than towards propylene was suggested to further increase the selectivity for acetone. Altogether, the incorporation of the catalyst into the membrane led to a considerable increase (around 14 times) of the acetone/propylene ratio as compared with the one reached in a fixed bed [58].

Parmaliana and co-workers have been studying the potentialities and the particular features of an innovative three-phase CMR for the selective oxidation of light alkanes into higher added value oxygenated products, using environmentally friendly superacid catalysts and the clean Me^{n+}/H_2O_2 Fenton system as oxidizing agent [60-66] (cf. Table 3). Indeed, the industrial processes for producing oxygenates, such as acetone, for example, imply the use of starting materials that are themselves intermediate products obtained from petrochemical processes and a series of reaction and separation units that limit the efficiency of the overall process. Thus, the development of a novel technology based on the three-phase CMR, which allows the one-step synthesis of oxygenates with simultaneous reaction and separation of the desired products, seems to be an interesting alternative for both the catalytic conversion of natural gas and light alkanes. The separation of intermediate products from the liquid phase

containing the oxidant is very effective in preventing their further oxidation and thus reaching high yields of partially oxidised light paraffins [66], particularly if hollow fibre (rather than flat sheet) membranes are used [64]. Additionally, coupling the *in situ* generation of H_2O_2 from H_2 and O_2 in catalytic polymeric membranes [71] with the alkanes oxidation could result in significant improvements of the process economics.

Other examples mentioned in Table 3 are the catalytic oxidation of sulphides [67], the catalytic oxidation of primary aliphatic alcohols (1-butanol, 1-hexanol) with air [68] and the oxidation of secondary amines to nitrones [69]. The one-step selective oxidation of benzene to phenol is also of concern, due to its relevance as chemical intermediate, although conversion levels are still low [70].

HYDRATION REACTIONS

There are a few examples of hydration reactions in which catalytic polymeric membranes have been used, namely the studies by Vital and co-workers on the acid catalysed hydration of α-pinene [72-75]. Initially, the main goal of these studies was to found the best reaction system and conditions to increase the conversion and selectivity towards terpenic alcohols, valuable products with many applications in the pharmaceutical industry, namely α-terpineol. The authors utilized different combinations of polymeric membrane/occluded catalysts (e.g. polydimethylsiloxane or polyvinyl alcohol membranes containing zeolite USY, zeolite beta, activated carbons, dodecamolybdophosphoric acid/USY or molybdophosphoric acid), and different liquid phase reactor arrangements (particularly batch and tubular reactors with interfacial contact, at 50-55 ºC). Through experiments made in many systems, they were able, in some cases, to improve the performance (activity and/or selectivity) of the MR as compared to that exhibited by the same catalyst in conventional reactors. For instance, as a result of the increase of the channelling network inside the membrane, due to the increase of the catalyst loading, the mass transfer resistance decreased. This led to a higher diffusion rate of the reagents to the catalyst particles and to an enhanced catalytic activity of the MR [74]. An important factor for higher catalytic activity is the hydrophobic character of the membrane [73, 74], which should be increased, up to a certain extent (therefore α-pinene diffusivity is also increased, and consequently its concentration near the active sites). However, in some cases this higher activity was not followed by an also higher selectivity, suggesting that a compromise between activity and selectivity could be obtained through the fine-tuning of the hydrophilic/hydrophobic balance [73]. These authors developed a kinetic-diffusion model with the purpose to describe the experimental results [72, 75], which is described below in detail (see section "*Liquid/Vapour Phase Membrane Reactors*").

Another example of a hydration reaction is the conversion of isobutene into *tert*-butyl alcohol (TBA) reported by Song and Lee [9]. The results showed that the catalytic membranes led to higher TBA yields than the homogeneous process, being, among the systems used (either polyphenylene oxide or polysulfone catalytic membranes operating in a semi-batch reactor), dodecamolybdophosphoric acid with the polyphenylene oxide membrane (HPMo-PPO) the most active one. This behaviour was connected with the absorption capability of the polymer materials for isobutene, showing that the polymer matrix is not a simple support for the HPMo catalyst, but served as an efficient reservoir for isobutene,

enhancing its concentration in the composite catalyst. This is very important to overcome the low solubility of isobutene in water that is encountered in a normal liquid phase TBA synthesis.

OTHER REACTIONS

Polymeric membrane-supported catalysts have also find application in other reaction systems. It is out of the scope of the present chapter to extensively review all such applications, so we will only mention briefly a few examples, where the interested reader can find much more information. Such examples of other (potential) applications include hydroformylation (reaction between a terminal olefin and syngas to give aldehydes) [76], isomerization [77], esterification [78-80], and dimerisation [81, 82] reactions, as well as the MTBE decomposition to yield high purity isobutene [83, 84]. In the particular case of esterification reactions, pervaporation (or vapour permeation) has often been associated with, in order to extract continuously one of the formed products (in this case water) to achieve complete conversion of the reactants. This assembly gained particular significance due to the industrial importance of esters. Several other examples of coupling pervaporation with chemical reactions have been previously mentioned [31, 32, 79, 80], but many others are pointed out in the review by Ozdemir *et al.* [1] who dedicate an entire section to that issue.

One application that is worth mentioning is the carbon monoxide elimination in streams fed to fuel cells (FCs). Actually, the conversion of fuels into hydrogen (for instance through steam-reforming) for FCs operation is of great interest. However, the carbon monoxide that is also produced has a detrimental effect because it poisons the catalyst in the FC. This way, the reaction between carbon monoxide and water to generate more hydrogen (and also carbon dioxide), the so-called water gas shift reaction (WGS), has a considerable interest. As the WGS reaction is equilibrium-limited, the product stream contains usually high concentrations of unconverted CO. Notwithstanding, the performance in this exothermic reaction can be enhanced significantly if a CO_2-selective and/or a H_2-selective membrane is used, shifting therefore the equilibrium towards the reaction products. In the case of H_2, Pd-based selective membranes have been traditionally used operating at temperatures around 300 °C. In the case of CO_2, two selective polymeric membranes have been reported recently [85, 86] and obtained by incorporating amino functional carrier groups [85, 87]. The membranes by Ho and co-workers [88] are reported to show a CO_2 permeance of ca. 20 $m^3_{STP}\,m^{-2}\,h^{-1}\,bar^{-1}$ at 140 °C and a CO_2/H_2 ideal selectivity of ca. 40. The second membrane showed a CO_2 permeance of ca. 0.1 $m^3_{STP}\,m^{-2}\,h^{-1}\,bar^{-1}$ at 35 °C and a CO_2/H_2 ideal selectivity of ca. 100 [89]. Moreover, a selectivity of 5 for CO_2/CO was also reported by the same authors also at 35 °C [89]. Ho and co-workers simulated the use of their membrane to work in a WGS membrane reactor, showing that it is possible to produce a hydrogen stream in the retentate side with less than 10 ppm of CO and a H_2 recovery greater than 97% [88, 90].

Also of concern is the reduction of nitrous oxide, reported by Fritsch and Peinemann [91] using homogeneous dense catalytic active membranes (poly(amide-imides)) with uniformly distributed ultrafine catalyst particles (e.g. Pd ~2 nm, with >20 wt.%).

Another interesting application of polymeric MRs is the vegetable oil (and/or animal fat) transesterification for the production of bio-diesel fuels. These are usually prepared by such

reaction with methanol in the presence of strong acids. Guerreiro *et al.* [92] have recently employed with success membranes with acidic properties to catalyse the soybean oil transesterification, at 60 ºC and atmospheric pressure. A remarkable performance of poly(vinyl alcohol) membranes modified with sulfosuccinic acid was recorded, attributed in part to their high content of sulfonic groups and swelling properties.

MODELLING OF POLYMERIC CATALYTIC MEMBRANE REACTORS

Modelling and simulation are key tools for better understanding the behaviour of a given system and for scale-up, optimization and control purposes. Modelling can also be used to conceive and study new processes at lower costs.

In order to model a membrane reactor with a catalytic membrane (CMR), at least three different regions must be considered: the retentate chamber, the catalytic membrane module and the permeate chamber. The governing mass, energy and momentum balance equations for each region are directly related with the assumptions considered and the operating conditions. For the retentate and permeate chambers, for example, there are two main aspects that must be considered: the flow pattern and the possible existence of mass transfer resistance at the fluid/membrane interface (the so-called concentration-polarization). Usually, for gas phase reactions, the flow pattern at the retentate and permeate chambers is considered to be perfectly mixed or plug flow; beyond these, it can also be considered a cross flow pattern at the permeate chamber. No pressure drop is usually considered at either chamber for gas-phase reactions. Concerning the interface bulk/membrane, it is usually assumed that the mass transfer resistance is negligible (no occurrence of concentration polarization). Regarding the catalytic membrane, a model for the mass transport and the corresponding equation(s) to describe the reaction rate(s) should be assumed.

For several reasons, almost only dense rubbery polymers have been used to synthesise polymeric catalytic membranes. The mass transport mechanism through such membranes has been assumed to follow the well-known sorption-diffusion model [93]. On the other hand, modelling the chemical reaction(s) inside the membrane is usually a much more complex problem. Basically, there are two approaches: in one of them, a specific chemical reaction is carried out in the catalytic membrane. A reaction rate model is assumed and the related parameters are determined by fitting the global model to the experimental data. This could be done by carrying out the chemical reaction under special operating conditions, e.g. in a batch reactor where the catalyst is dispersed in a support [24, 25] or directly in the catalytic membrane [11, 72, 75, 77], or simply using the kinetic models determined by other authors [56, 94]. In the other approach, a theoretical reaction rate model and the respective model parameters are assumed [95-104].

The interest in modelling and simulating CMRs has increased considerably in the past few years. However, almost all the work has been focused in inorganic membrane reactors, as it can be realized throughout other chapters of this book. The studies about modelling and simulation of membrane reactors with polymeric catalytic membranes are very limited in number and nature. In the following sections, some examples available in the literature are going to be presented and discussed. These works are organized in two different categories according to the nature of the feed and exit streams: **liquid/vapour-phase PCMRs** or **gas-**

phase PCMRs. We will focus specifically in membrane reactors with polymeric catalytic membranes. The examples that deal with membrane reactors with polymeric non-catalytic membranes are usually related with different subjects, namely bio-reactors, photocatalysis and others (discussed in different chapters of the present book). In the case of packed-bed membrane reactors with polymeric non-catalytic membranes, where the specific function of the membrane is only the separation, the models are similar to the ones devoted to inert inorganic membranes, which are widely covered and discussed in other chapters of the present book. The only difference between both types of membranes is the transport equation for the reaction species.

LIQUID/VAPOUR PHASE MEMBRANE REACTORS

Yawalkar *et al.* [94] developed a one-dimension mathematical model to describe theoretically the steady-state liquid phase epoxidation of alkenes to epoxides in a CMR. The model's emphasis was put on the effect that some variables and parameters had on the membrane reactor performance, namely the peroxide and alkene concentrations in the liquid phase, the peroxide and alkene sorption coefficients and the catalyst particles loading and size. The reactor was operated in interfacial contact mode (segregated feed of the reactants to each side of the membrane), with homogeneous concentration in both bulk organic and aqueous phases (well-stirred chambers) and in conditions such that there was no concentration polarization. The main assumptions of the model considered by the authors were the following:

- The catalytic membrane consisted of a homogeneous polymeric phase with cubic zeolite catalyst particles, all of the same size, built-in and distributed uniformly throughout, *i. e.*, the distance between successive particles was the same.
- Membrane partition coefficients for the peroxide and organic phases were assumed to be independent of each other.
- The authors considered two simultaneous reactions to describe the alkene epoxidation: the epoxidation reaction itself, between the peroxide and the alkene to give epoxide and by-products, and the side undesirable peroxide decomposition.
- Due to the organophillic nature of the membrane, the concentration of alkene inside the membrane was assumed to be much higher than that of the peroxide. In this way, the epoxidation reaction was considered to be of pseudo first order concerning the peroxide concentration.
- The proposed model considered fickian diffusion of the reactant peroxide in the polymeric phase and in the catalyst particles.
- Membrane partition coefficients of peroxide between the bulk liquid phase and the membrane surface, as well as between the polymer phase and the catalyst surface, were assumed to be described by the Henry's law.

According to these simplifications, the model equations consist of the fickian mass transport of peroxide across the polymeric phase as well as the fickian mass transport and reaction across the catalyst particles. The boundary conditions include the sorption equilibrium for the interfaces gas/polymer and polymer/catalyst (described by Henry's law) and equality of fluxes at the interfaces polymer/catalyst.

The model predictions showed how the organophillic membrane phase, along with the zeolite particles, lowered the excess of peroxide at the catalyst active sites, thus reducing drastically its decomposition and the catalyst deactivation. By proper selection of the various parameters, high peroxide efficiency and significant rate of epoxide generation could be obtained.

The Yawalkar's model was extended very recently by Nagy [95]. The author used a simple physical model for the distribution of the catalyst particles inside the membrane layer, as well as for the mass transport throughout it, and studied the influence of some membrane properties, such as the size and geometric distribution of the catalyst particles, the catalyst phase hold-up, the distance of the first catalyst particle from the membrane surface and the membrane thickness, as well as the diffusion coefficients in the membrane phase and in the catalyst particles. A chemical irreversible first-order reaction occurring inside the catalyst particles was considered, although the developed methodology could also be extended for higher-order chemical reactions. Depending on the particle size, the author considered two different models: a pseudo-homogeneous one, suitable to be applied when the size of the catalyst particles was very low (submicrometer-sized), and a heterogeneous model, recommended for larger particles (several micrometers in size). Specifically for the case of first order irreversible reactions, the author developed analytical mathematical equations for the prediction of the mass-transfer rates as a function of every physical and chemical parameters that characterizes the catalytic membrane layer, namely the diffusion and solubility coefficients, reaction rate constant, catalyst particle size, particle hold-up and membrane thickness. One of the main conclusions from that study was that the mass-transfer rate could be significantly improved by decreasing the size of the catalyst particles and the distance between the first particle and the membrane surface. On the other hand, the low diffusion coefficient through the catalytic particles, which is very often the case, could strongly lower the global mass-transfer rate, as well as the effect of the chemical reaction on it.

Kaliaguine and co-workers [56] studied and modelled a similar catalytic membrane reactor used in the oxyfunctionalization of *n*-hexane with hydrogen peroxide into a mixture of hexanols and hexanones, as mentioned above (Table 3). The authors used a solvent-free biphasic liquid-vapour catalytic polymeric membrane reactor operating in interfacial contact mode, where the catalytic membrane was a composite PDMS polymer built-in with titanium silicalite zeolite TS-1. The authors developed a simple steady-state diffusion-reaction model for describing the reactants concentration profiles and oxygenates formation rates inside the membrane based on the following main assumptions:

- Isothermal and isobaric reaction conditions.
- Mass transport of the reactants truly unidirectional, that is, occurring only through the membrane thickness (this is generally the case, as the membrane thickness is usually much smaller than its surface area), and described by the Fick's law.

- Homogeneous and isotropic membrane, with the reactants concentration in the liquid aqueous (H_2O_2) and vapour organic (*n*-hexane) phases in equilibrium with the ones at the respective membrane surface.
- Diffusion coefficients independent of the concentration, that is, constant throughout the membrane thickness.
- Independence of the reaction rate relatively to the internal mass transfer resistance (diffusion) in the catalyst particle, that is, particle effectiveness factor close to unity.
- No boundary layer on the membrane surfaces, that is, no mass transfer resistance for the reactants and reaction products at the interface membrane surface/bulk phase solution.
- Effective (experimental) values for the partition coefficients of peroxide (interface membrane/aqueous phase) and *n*-hexane (interface membrane/organic phase). The solubility of each of these components in the other phase was assumed to be negligible.
- Negligible concentration of the reaction products in both membrane surfaces, that is, as these species reach the membrane surface, they are immediately separated from it, due to their immiscibility in the bulk liquid/vapour phases.

According to these simplifications, the model equations consisted of the mass transport (fickian) and reaction balances for all the reaction species. The respective simulations showed to describe accurately the average formation rates of the oxygenate species, which were found to fit quite well with the ones obtained from the experiments. They demonstrated also that the hydrogen peroxide diffusivity in the catalytic polymeric membrane had a strong effect on the rates of oxygenates formation (the reaction was conducted in an excess of *n*-hexane). The authors still evidenced the feasibility of the principle of using a catalytic membrane as interphase contactor in a biphasic reaction. Specifically for this system, the catalytic membrane was effective not only in the production of hexanols and hexanones, but also in the separation of these products from the organic feed. Despite the authors discussed the influence of the catalyst loading and the membrane modifications on the catalytic performance, the presented results showed only the influence of the hydrogen peroxide diffusivity. A simple numerical example based in this model and solved using the software MADDONA will be presented later in the section "*Appendix: Examples of Application Using Madonna*".

Vital and co-workers [75] also developed a simple model to describe the hydration of α-pinene into α-terpineol and a series of other products, being the reaction carried out in a batch catalytic polymeric membrane reactor. The catalytic membrane was a composite PDMS polymer built-in with zeolite USY 750 as catalyst. The reactant solution used was a mixture of water and α-pinene in acetone (as solvent). The authors developed a simple transient model to describe the reactants and reaction products concentration as a function of time in the reactor chamber, which was developed based on the following main assumptions:

- Isothermal and isobaric reaction conditions.
- Pseudo steady-state conditions for diffusion and reaction inside the membrane.

- Mass transport of the reactants inside the membrane truly unidirectional and described by the Fick's law, as also assumed in the Kaliaguine's model [56].
- Homogeneous and isotropic membrane macrostructure, as also assumed by Kaliaguine *et al*. [56].
- Equilibrium concentration of the reactants in the liquid phase with the one in the membrane surface, described by a linear relationship (Henry's law).
- No mass transport resistance for the reactants from the solution bulk phase to the membrane surfaces (no concentration polarization effect).
- The diffusivity of α-pinene was assumed to be independent of its own concentration, but considered to depend on the concentration of α-terpineol.
- Independence of the observed reaction rate relatively to the internal diffusion in the catalyst particle (zeolite).
- Consumption of the α-pinene reactant (species *A*) according to a parallel reaction network. The reaction product α-terpineol (species *B*) was considered to not react subsequently. A series of the others components were lumped into a generic component (species *C*).
- Since the sorption of water in a PDMS membrane is low and there is a large excess of this reactant relatively to α-terpineol, the authors assumed a pseudo first order elementary reaction rate for the two parallel reactions.

According to these simplifications, the model equations considered the mass balance equation for component *A* inside the membrane at pseudo steady-state conditions (fickian transport and reaction rate) and the mass balances in the reactor chamber for components *A*, *B* and *C* at transient conditions. The reactor was operated in total recycle mode. The results obtained with this model showed to describe quite well the average concentration history of reactants and reaction products in the liquid phase, as well as the selectivity to α-terpineol. The model predicted also the increase of the reactants permeability as a function of the catalyst loading.

In a later work by this group [72], the authors applied a similar model to the same reaction system, but now conducted over molybdophosphoric acid immobilized in hydrophobic polyvinylalcohol membranes modified with acetic anhydride. In that study, the authors considered a slightly more complex model to describe the parallel chemical reaction network: a second order elementary reaction rate for the reaction concerning the production of α-terpineol and a first order elementary reaction rate for the secondary (parallel) reaction. Like in the previous work [75], the model proved to describe reasonably the obtained experimental results.

Frisch *et al.* studied the dehydrogenation of cyclohexane to benzene [11] and the *cis* to *trans* isomerization of piperylene [77], both carried out in a batch catalytic polymeric membrane reactor at low temperature. The catalytic membrane was a composite polyethylacrylate polymer built-in with a zeolite 13X containing a catalyst based on Ni or Ti [11] and on Co [77]. The feed to the membrane consisted of pure reactants in vapour phase. In order to calculate the reaction rate constants and the activation energies in both studies, the authors developed and solved a simple transient diffusion-reaction model, considering pseudo first order reaction relatively to the reactants. The diffusion coefficient of the reactants in the membranes, necessary to solve their model, was obtained by the time-lag method using

control membranes, that is, membranes containing the same zeolite 13X, but free of catalyst. The calculated values were consistent with kinetics controlled by the surface diffusion.

GAS PHASE MEMBRANE REACTORS

Modelling and simulation of polymeric catalytic membrane reactors for carrying out gas phase reactions is a subject that has been deserved some attention mainly by our research group, conducting either theoretical [96-104] or experimental studies [24, 25].

Various studies are now going to be presented, following the relevant publications. First of all, it will be described an isothermal reactor for conducting equilibrium-limited gas phase reactions with perfectly-mixed flow pattern. Then, a different flow pattern, the plug flow, will be introduced and discussed, keeping, though, the same reaction type. Finally, a nonisothermal reactor applied for conducting a consecutive-parallel gas phase reaction system, also with perfectly-mixed flow pattern, will be introduced and discussed.

Isothermal/perfectly-mixed flow pattern models.

Concerning the theoretical aspects, the first model developed for gas phase catalytic membrane reactors considered an equilibrium-limited reaction of the type $aA + bB \underset{k_i}{\overset{k_d}{\rightleftarrows}} cC + dD$ occurring in a polymeric catalytic nonporous membrane reactor (PCMR) with nanosized catalyst distributed homogeneously across the membrane, as sketched in Figure 1 [96, 97].

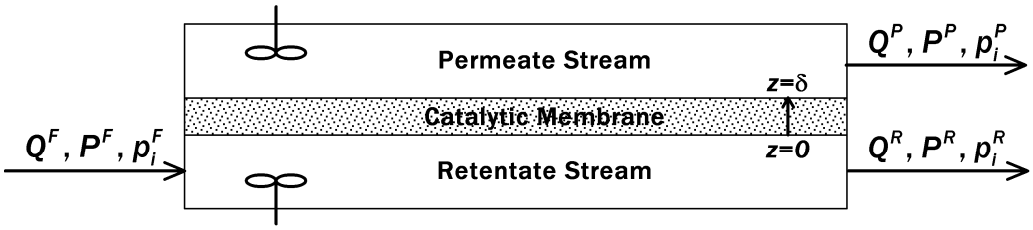

Figure 1. Schematic diagram of the polymeric catalytic membrane reactor (PCMR). Adapted from [96].

This model was developed based on some assumptions, which will be described along the text when the presentation of the respective mathematical equations. These equations comprise the steady-state differential mass balance for the membrane in planar coordinates and the respective boundary conditions, as well as the algebraic mass balances for the upstream and downstream chambers.

MASS BALANCE AND BOUNDARY CONDITIONS FOR THE MEMBRANE

$$D_i \frac{d^2 c_i}{dz^2} + \nu_i k_d f(c_i) = 0 \quad (1)$$

The first term describes the diffusive transport through the membrane and the second one describes the chemical reaction. The main assumptions considered in this model are: steady-state and isothermal conditions, transport of the reaction species throughout the membrane described by the sorption-diffusion model, fickian diffusion, and constant sorption and diffusion coefficients throughout the membrane and for the whole range of concentrations. Symbol i refers to the i^{th} component, D is the diffusion coefficient, c is the concentration inside the membrane, z is the spatial coordinate perpendicular to the membrane surface, ν is the stoichiometric coefficient (taken positive for products and negative for reactants), k_d is the direct reaction rate constant and f is the local reaction rate function, defined as follows:

$$f(c_i) = \frac{1}{k_d}\left(k_d (c_A)^a (c_B)^b - k_i (c_C)^c (c_D)^d\right) = \left((c_A)^a (c_B)^b - \frac{(c_C)^c (c_D)^d}{k_d / k_i}\right) = \left((c_A)^a (c_B)^b - \frac{(c_C)^c (c_D)^d}{R_k}\right) \quad (2)$$

It was considered an elementary reaction rate law and that such reaction occurred only at the surface of the nanosized catalyst particles. It was still assumed that the concentration of the reaction species (at the catalyst surface) was equal to the local concentration on the polymer phase. In principle, any relationship could be considered for this partition coefficient, but this one simplifies the original problem without compromising the main conclusions. Symbol k_i is the reverse reaction rate constant and R_k is the ratio between the direct and reverse reaction rate constants, that is, an equilibrium constant. Sousa *et al.* [96, 97] considered this parameter equivalent to the thermodynamic equilibrium constant based on the gas phase feed conditions, K_e. However, this assumption is only strictly valid when activity coefficients are unitary, which was assumed by the authors [96, 97]. More generally, the equilibrium constant obtained from the concentration ratio between products and reactants is different when considering the gas and membrane phases. In this way, the sorption-based enhancement of the equilibrium conversion reported by Sousa *et al.* [96, 97] is not generally valid.

The second order differential equation (1) needs two boundary conditions, in this case an equilibrium condition at the interfaces membrane/gas:

$$\text{At } z = 0 \text{ (retentate side)}, \; c_i = S_i p_i^R \quad (3)$$

$$\text{At } z = \delta \text{ (permeate side)}, \; c_i = S_i p_i^P \quad (4)$$

It was assumed that such equilibrium condition is described by the Henry's law and also that there was no external mass transport limitations in the interface (no occurrence of concentration polarization). Symbol p represents the partial pressure in the bulk gas phase and the superscripts R and P refer to the retentate and permeate stream conditions, respectively. δ represents the membrane thickness and S represents the membrane partition coefficient between the bulk gas phase and the membrane surfaces.

PARTIAL AND TOTAL MASS BALANCES FOR THE RETENTATE CHAMBER

It was assumed perfectly-mixed flow pattern with negligible drop in the total pressure and ideal gas behaviour in the development of the mass balances for the retentate chamber. The corresponding mathematical equations are:

$$\frac{Q^F p_i^F}{\Re T^F} - \frac{Q^R p_i^R}{\Re T^R} + A^m D_i \left.\frac{dc_i}{dz}\right|_{z=0} = 0 \tag{5}$$

$$\frac{Q^F P^F}{\Re T^F} - \frac{Q^R P^R}{\Re T^R} + A^m \sum_i D_i \left.\frac{dc_i}{dz}\right|_{z=0} = 0 \tag{6}$$

The first and second terms of these equations describe the molar flux that comes into and out of the reactor on the retentate side, respectively. The third term describes the molar flux exchanged between the membrane and the retentate chamber. Symbol Q is the volumetric flow rate, P represents the total pressure, A^m is the membrane surface area, $\Re$ is the universal gas constant and T is the absolute temperature. The superscript F refers to the feed stream conditions.

PARTIAL AND TOTAL MASS BALANCES FOR THE PERMEATE CHAMBER

In the development of these mass balances, it was also assumed perfectly-mixed flow pattern with negligible drop in the total pressure and ideal gas behaviour. The corresponding equations are now:

$$\frac{Q^P p_i^P}{\Re T^P} + A^m D_i \left.\frac{dc_i}{dz}\right|_{z=\delta} = 0 \tag{7}$$

$$\frac{Q^P P^P}{\Re T^P} + A^m \sum_i D_i \left.\frac{dc_i}{dz}\right|_{z=\delta} = 0 \tag{8}$$

By analogy with the retentate chamber, the first term describes the molar flux that comes out of the reactor by the permeate side and the second term describes the molar flux exchanged between the membrane and the permeate chamber.

Equations (1)-(8) were made dimensionless, becoming as follows:

$$D_i^* \frac{\mathrm{d}^2 c_i^*}{\mathrm{d}\zeta^2} + \nu_i \Phi^2 f(c_i^*) = 0 \tag{9}$$

$$f(c_i^*) = \left[(c_A^*)^a (c_B^*)^b - (c_C^*)^c (c_D^*)^d \frac{(C_{ref})^{\Delta n}}{K_e} \right] \tag{10}$$

$$\zeta = 0, \quad c_i^* = S_i^* p_i^{R*} \tag{11}$$

$$\zeta = 1, \quad c_i^* = S_i^* p_i^{P*} \tag{12}$$

$$Q^{F*} p_i^{F*} - Q^{R*} p_i^{R*} + \Gamma D_i^* \left. \frac{\mathrm{d}c_i^*}{\mathrm{d}\zeta} \right|_{\zeta=0} = 0 \tag{13}$$

$$Q^{F*} P^{F*} - Q^{R*} P^{R*} + \Gamma \sum_i D_i^* \left. \frac{\mathrm{d}c_i^*}{\mathrm{d}\zeta} \right|_{\zeta=0} = 0 \tag{14}$$

$$Q^{P*} p_i^{P*} + \Gamma D_i^* \left. \frac{\mathrm{d}c_i^*}{\mathrm{d}\zeta} \right|_{\zeta=1} = 0 \tag{15}$$

$$Q^{P*} P^{P*} + \Gamma \sum_i D_i^* \left. \frac{\mathrm{d}c_i^*}{\mathrm{d}\zeta} \right|_{\zeta=1} = 0 \tag{16}$$

where

$$c_i^* = c_i / C_{ref}, \qquad P^* = P / P_{ref}, \qquad p_i^* = p_i / P_{ref}, \qquad D_i^* = D_i / D_{ref},$$

$$Q^* = Q / Q_{ref}, \qquad S_i^* = S_i / S_{ref}, \qquad \zeta = z / \delta, \qquad \Delta n = c + d - a - b$$

$$\Phi = \delta \left(\frac{k_d \left(C_{ref} \right)^{a+b-1}}{D_{ref}} \right)^{1/2}, \qquad \Gamma = \frac{A^m D_{ref} C_{ref} \Re T}{\delta Q_{ref} P_{ref}} = \frac{A^m D_{ref} S_{ref} \dfrac{P_{ref}}{\delta}}{\dfrac{Q_{ref} P_{ref}}{\Re T}}$$

The total feed pressure and total feed volumetric flow rate were taken as reference conditions to define the dimensionless pressure and volumetric flow rate, respectively. Species *A* was taken as the reference component to define the dimensionless diffusion and sorption coefficients and C_{ref} was defined as the reference concentration ($C_{ref} = S_{ref} P_{ref}$). The set of dimensionless equations contains two dimensionless groups: the Thiele modulus, Φ, which represents the ratio between the characteristic intramembrane diffusion time for the reference component and the characteristic direct reaction time, and a dimensionless contact time, Γ, which represents the ratio between the maximum possible flux through the membrane for the reference component, that is, permeation of pure species against null permeate pressure, and the total molar feed flow rate (see the respective mathematical definitions above). This last parameter is somehow related with the stage-cut, that is, the feed fraction that permeates through the membrane. For the case of 100 % stage-cut, the reactor operates in what is called "total flow-through configuration" or in "dead-end flow" [105].

Due to the characteristics of the membrane reactors, it is expected that, in some way, they perform better than a conventional reactor. In these specific studies [96, 97], the main objective of the authors was to compare the performance of the catalytic polymeric membrane reactor with the more conventional counterpart catalytic reactor exclusively in terms of the achieved conversion for an equilibrium-limited gas phase reaction. More specifically, they studied the role played by the different diffusivity and sorption selectivities for the reaction species on the performance of a catalytic polymeric membrane reactor.

"Conventional", in the context of their work, meant a catalytic reactor operating in similar conditions as the ones of the catalytic membrane reactor, that is: the same flow pattern (perfectly-mixed), fed with a gaseous mixture in the same conditions of composition and pressure, containing the same catalyst and with the same chemical reaction taking place at the catalyst surface. Additionally, the chemical reaction was considered to be described by equivalent kinetic equations in both reactors and with the same ratio between the direct and reverse reaction rate constants, that is, with the same equilibrium constant. At last, it was assumed that the maximum conversion achieved in the conventional catalytic reactor was the thermodynamic equilibrium value, being then its equilibrium constant value the thermodynamic equilibrium one. Through this assumption, the conversion achieved in the catalytic membrane reactor was compared with the thermodynamic equilibrium value. To perform such an analysis, it was considered the variable "*relative conversion*", Ψ_A, defined as the ratio between the conversion of the reactant *A* attained in the membrane reactor, X_A, and the thermodynamic equilibrium conversion based on the gas phase feed conditions, X_A^E. The conversion reached in the membrane reactor was calculated by the following equation:

$$X_A = \frac{\dfrac{Q^F p_A^F}{\Re T} - \left(\dfrac{Q^R p_A^R}{\Re T} + \dfrac{Q^P p_A^P}{\Re T} \right)}{\dfrac{Q^F p_A^F}{\Re T}} = 1 - \frac{Q^{R^*} p_A^{R^*} + Q^{P^*} p_A^{P^*}}{Q^{F^*} p_A^{F^*}} \qquad (17)$$

The numerical details concerning the resolution of the model equations are described below, in the section "*Numerical Methods for Membrane Reactors*".

RESULTS AND DISCUSSION

In the studies by Sousa *et al.*, [96, 97], several simulations were performed in order to understand how the relative conversion depended on the dimensionless contact time and Thiele modulus parameters for different dimensionless diffusion and sorption coefficients of the reaction components and for different reaction stoichiometries. From the set of the respective results, the authors concluded that it is possible to reach conversions higher than the thermodynamic equilibrium value, for a given set of conditions. This conversion enhancement could be obtained, for example, by selecting a membrane where the diffusion coefficients of the reactants are lower than the ones of the reaction products. These conclusions can be observed in Figure 2, where the relative conversion of a PCMR is presented as a function of the dimensionless contact time and for different Thiele modulus

values. The relevant variables are: $D_B^* = 0.1$, $p_A^{F*} = 0.5$, $p_B^{F*} = 0.5$, $p_C^{F*} = 0$, $p_D^{F*} = 0$, $K_e = 0.1$, $\nu_i = 1$ and $P^{P*} = 0.01$ [96].

This figure show a continuous increase of the conversion with the contact time until the reactor operates in the total flow-through configuration, also named as "total permeation condition", *TPC* (described by the line *TPL* in the figure). That is, the maximum conversion is attained when the reactor operates in conditions of no reactants loss on the retentate stream and where the reacting species have the longest possible contact with the catalyst inside the membrane. The maximum value of the contact time parameter (at the *TPC*) for each Thiele modulus depends on the pressure difference between both sides of the membrane, for a given set of sorption and diffusion coefficients values.

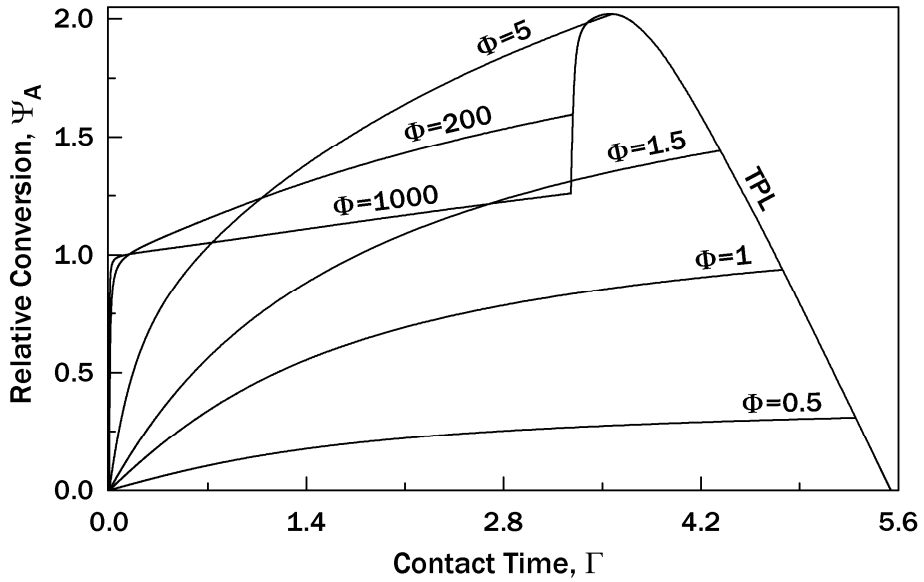

Figure 2. Relative conversion of component A as a function of the dimensionless contact time for various Thiele modulus values. $D_B^* = 0.1$, $D_{i \neq B}^* = 1$ and $S_i^* = 1$. The other variables have the values referred in the text.

Due to the higher average reaction products permeability than the one of the reactants, and according to the *Le Chatelier* principle, the local chemical reaction condition inside the membrane, that is, the ratio $\frac{\left(c_C^*\right)^c \left(c_D^*\right)^d}{\left(c_A^*\right)^a \left(c_B^*\right)^b} \left(C_{ref}\right)^{\Delta n}$ [97], defined as the *chemical reaction coefficient*, Θ (see equation (10)) goes beyond the thermodynamic equilibrium value in a fraction of the membrane thickness on the downstream side (see Figure 3). As a result, the chemical reaction is shifted favourably towards the reaction products and the chemical conversion increases beyond the thermodynamic equilibrium value (Figure 2).

This displacement of the local chemical equilibrium condition arises from the net balance between the separation effect (which shifts the reaction to the right side) and the backward reaction effect (which tries to hinder such shifting) and depends directly on the Thiele

modulus value. That is, for low values of this parameter (Φ<5 in the example presented in Figure 2), the characteristic reaction time overlaps the characteristic diffusion time (the reactor operates in the so-called chemical controlled regime) and then the backward reaction effect is incipient, resulting in an effective chemical reaction shifting towards the reaction products, as can be observed in Figure 3. In this region, the chemical conversion increases continuously with the Thiele modulus and contact time parameters, as the catalyst is more and more effectively used. As the Thiele modulus increases more and more, the ratio of the characteristic times is inverted and the reactor becomes to operate in the so-called diffusional controlled regime. The equilibrium shift due to the preferential diffusion of the reaction products is now more and more cancelled out by the backward reaction, resulting in a decrease of the reactor conversion enhancement. In fact, the separation effect is more and more restricted to a narrower region of the membrane thickness on the downstream side (Figure 3). The limit conversion for an instantaneous reaction (very high Thiele modulus) should approach the thermodynamic equilibrium value (Figures 2 and 3).

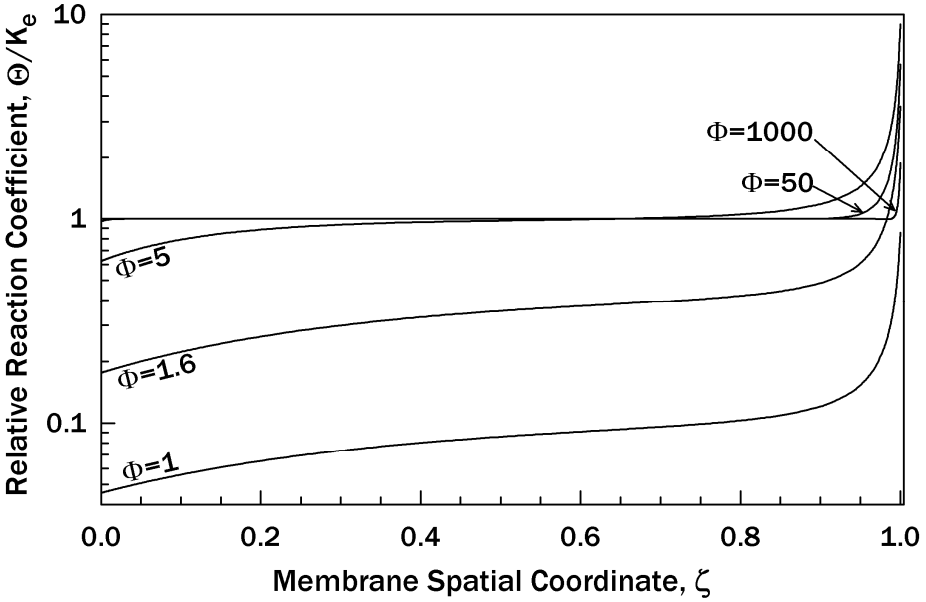

Figure 3. Relative reaction coefficient at the TPC as a function of the dimensionless spatial coordinate in the membrane for various Thiele modulus values. Same variable values as in Figure 2.

Finally, Figure 2 shows two different behaviours for the evolution of the contact time at the total permeation condition with the Thiele modulus value: one region where a more or less fast decrease occurs, from the low Thiele modulus values until the maximum conversion is attained, following a second region of a considerably slower decrease. The decrease of the contact time parameter (related with the reactor size) with the increase of the conversion for low to medium Thiele modulus values (first region) is a consequence of the increase of the reaction components average permeability, that is, the chemical reaction transforms slower species (reactant B) in faster components (reaction products). In other words, the average residence time of the reaction species decreases with the Thiele modulus. For medium to high Thiele modulus values, the conversion decreases as explained above, however without a

consequent increase on the contact time parameter. This apparently contradictory behaviour occurs because it reflects the balance of two opposite trends: decreasing the conversion leads to an increase of the dimensionless contact time, that is, the reaction transforms now globally faster species (reaction products) into globally slower ones (reactants), increasing thus its average residence time; on the other hand, an increase of the Thiele modulus value leads the locus inside the membrane where the chemical equilibrium condition is attained to move towards the upstream and downstream membrane surfaces. According to Figure 3, the front of the local chemical equilibrium inside the membrane on the upstream side for this parametric region of the Thiele modulus is virtually at the membrane surface, changing only a little with the Thiele modulus in a narrow fraction of the membrane surface at the downstream side. Thus, the averaged concentration of the faster reaction species inside the membrane increases with the Thiele modulus, leading to a decrease of the average residence time of the reaction species, and, consequently, to a decrease of the contact time parameter. As a consequence, the transport of the reaction components through the membrane is more and more independent of the conversion in this parametric region.

The relative conversion of a PCMR as a function of the dimensionless contact time and for different Thiele modulus values for the case where $D_B^* = 10$ is presented in Figure 4. The other relevant variables are the same as in the previous case.

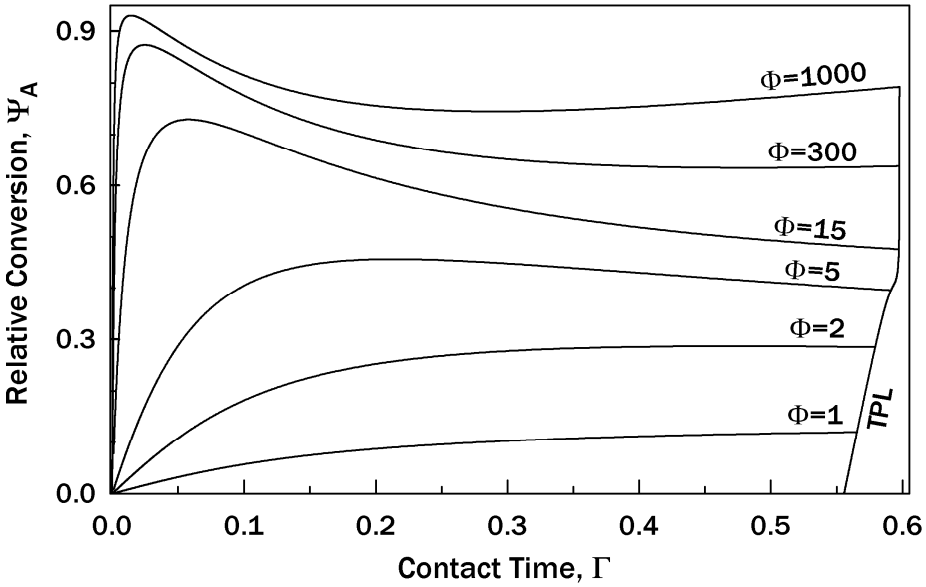

Figure 4. Relative conversion of component A as a function of the dimensionless contact time for various Thiele modulus values. $D_B^* = 10$, $D_{i\neq B}^* = 1$ and $S_i^* = 1$. The other variables have the same values as in Figure 2.

In this example, the average residence time of the reaction species inside the membrane increases with the Thiele modulus value, that is, with the conversion, because the chemical reaction transforms now globally faster species (reactants) into globally slower species (reaction products). As a consequence, the contact time at the total permeation condition

increases (and so the reactor's size too). However, there is a Thiele modulus value from which the contact time at the *TPC* remains approximately constant.

The separation effect discussed in the previous example (sowed in Figure 2) leaded the local chemical reaction condition inside the membrane to go beyond the thermodynamic equilibrium state in a fraction of the membrane thickness on the downstream side, according to the *Le Chatelier* principle (see Figure 3). In the present case, the separation effect has the opposite consequence, that is, it pulls down the local chemical reaction coefficient, Θ, in the same fraction of the membrane thickness closer to the downstream, which means that the chemical reaction condition is under the equilibrium state (see Figure 5). As the Thiele modulus value increases, this effect is gradually cancelled out, leading the locus inside the membrane where the chemical equilibrium condition is attained to move towards the upstream and downstream membrane surfaces, promoting a more and more effective use of the catalyst (increase of the conversion). As a consequence, the transport of the reaction components through the membrane is more and more independent of the conversion in this parametric region, and so it is also the contact time parameter.

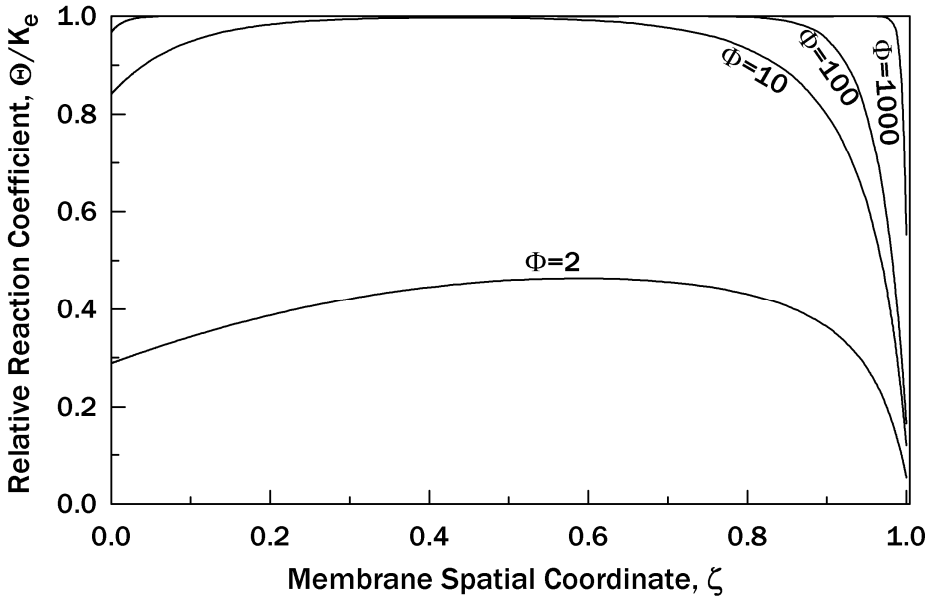

Figure 5. Relative reaction coefficient at the TPC as a function of the dimensionless spatial coordinate in the membrane for various Thiele modulus values. Same variable values as in figure 4

Contrarily to Figure 2, the maximum conversion is not attained anymore at the total permeation condition, for Thiele modulus values over a threshold one, but for lower values of the contact time parametric space. Such behaviour is primarily a consequence of the balance between two opposite effects: for a chemical controlled regime operation, that is, for low Thiele modulus values, the time of contact between the reactants and the catalyst is the most important factor and the conversion increases continuously with the contact time until the *TPC*. On the other hand, and due to the separation effect, the concentration of the faster permeating reactant (species B) in the retentate stream decreases with the dimensionless contact time, for a given Thiele modulus value, leading thus to a decrease of the reaction rate

and, consequently, of the reactor conversion (remember that the reactor conversion is analysed for reactant A). As soon as the reactor begins to work in the diffusional controlled regime, this separation effect becomes more and more important, and so the usage of the catalyst is maximized for lower and lower values of the contact time parameter. In this case, the maximum conversion is attained for a contact time lower than the value at the TPC (smaller reactor size), but there is a considerable loss of reactant on the retentate stream.

As expected, and contrarily to what is shown in Figure 2, the reactor conversion is under the thermodynamic equilibrium value when the diffusion coefficients of the reaction products are lower than the ones of the reactants (Figure 4). However, as the Thiele modulus value increases, the separation effect shown in both cases (Figures 2 and 4) is more and more cancelled out and the limit conversion attained in the reactor for an instantaneous reaction should be the thermodynamic equilibrium one.

The results just discussed are still influenced by the reaction stoichiometry, total pressure difference between the upstream and downstream chambers and the average concentration of reaction species inside the membrane [97]. For a chemical equilibrium limited reaction with $\Delta n=0$, the change of the global concentration of the reaction medium has no any influence on the conversion. However, for a membrane reactor where a chemical reaction with $\Delta n\neq 0$ takes place, the reactor conversion can be changed by tuning the average concentration of the reaction species inside the membrane (C_{ref}) and the total pressure difference between the retentate and the permeate chambers. For a chemical reaction with $\Delta n>0$, for example, the conversion can be favoured by a lower concentration in the reaction medium [97]. This can be achieved with a low C_{ref} value (that is, using a membrane with low affinity for the reaction components) and/or with a high pressure difference between the upstream and the downstream sides. This explains why the reactor conversion increases continuously with the contact time until the *TPC*, whichever is the Thiele modulus: in this condition, all the reactants must cross the membrane and the conversion is defined by the downstream conditions (low pressure) [97]. For a chemical reaction with $\Delta n<0$, on the other hand, the results are reversed [97]. In this case, such behaviour is the exclusive result of the manifestation of the *Le Chatelier* principle.

Isothermal/plug flow pattern models.

In the model described above, the flow pattern was considered to be perfectly mixed in both retentate and permeate chambers. In later works, that model was extended to include plug flow pattern in both retentate and permeate chambers, considering different flow configurations (co-current, counter-current and cross flow arrangement), as well as different feed configurations (through the tube side or through the shell side) [99, 100, 102]. The sketch of the catalytic membrane reactor for this model, fed through the tube side and operating in co-current flow, is presented in Figure 6.

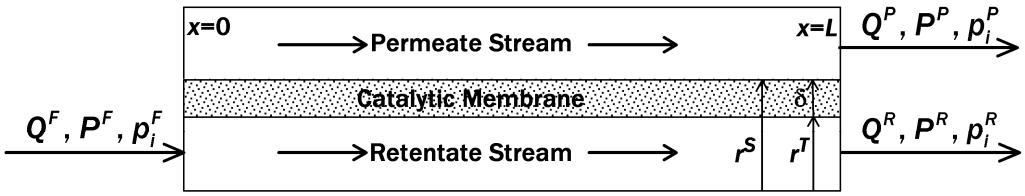

Figure 6. Schematic diagram of the dense catalytic tubular membrane reactor (for co-current flow and tube side feed). Adapted from [99].

This scheme represents cylindrical tube and shell chambers at different (but constant) total pressures P^T and P^S, respectively, separated by a cylindrical catalytic membrane of thickness δ and filled with a hypothetical nanosized catalyst homogeneously distributed throughout it. The reaction considered in this model was simpler than the one considered in the previous model, being now $aA \rightleftarrows bB$. The authors chose this hypothetical equilibrium reaction, where *A* and *B* represent the reactants and products, respectively, because the model proposed has an analytical solution for the membrane mass balance equations, for the case where a=b=1, allowing thus for a more accurate and faster solution of the global model, although without compromising the main conclusions.

The mathematical equations for this model comprise the steady-state second order diffusion/reaction differential mass balance for the membrane in cylindrical coordinates and the first order convection differential mass balances for the retentate (upstream) and for the permeate (downstream) chambers, as well as the respective boundary conditions.

MASS BALANCE AND BOUNDARY CONDITIONS FOR THE MEMBRANE

$$D_i\left(\frac{d^2c_i}{dr^2}+\frac{1}{r}\frac{dc_i}{dr}\right)+\nu_i k_d f(c_i)=0 \tag{18}$$

The meaning of the equation terms is the same as the one described for equation (1), as well as the main assumptions. Symbol *r* represents the radial coordinate perpendicular to the membrane surface. The other symbols were already defined and can be checked in the nomenclature section. The corresponding local reaction rate function, *f*, is defined as follows:

$$f(c_i)=\left((c_A)^a-\frac{(c_B)^b}{k_d/k_i}\right)=\left((c_A)^a-\frac{(c_B)^b}{R_k}\right) \tag{19}$$

As in the previous model, it was also considered an elementary reaction rate law, as well as the remaining main assumptions.

The second order differential equation (18) needs two boundary conditions, which describe the equilibrium condition at the membrane surface/bulk gas interfaces.

Considering tube side feed:

At $r=r^T$ (tube side, retentate chamber), $c_i = S_i p_i^R(x)$

(20)

At $r=r^S$ (shell side, permeate chamber), $c_i = S_i p_i^P(x)$ (21)

Like in the previous model, such equilibrium condition was assumed to be described by the Henry's law and no external mass transport limitations in the interface membrane/gas were also considered. r^T and r^S are the internal (tube side) and external (shell side) membrane radius and x is the axial coordinate along the reactor length. The other symbols were already defined and are described in the nomenclature section. Considering shell side feed, the equations are reversed.

MASS BALANCES AND BOUNDARY CONDITIONS FOR THE RETENTATE SIDE

$$\frac{1}{\Re T}\frac{\mathrm{d}\left(Q^R p_i^R\right)}{\mathrm{d}x} - 2\pi r^R D_i \left.\frac{\mathrm{d}c_i}{\mathrm{d}r}\right|_{r=r^R,x} = 0 \tag{22}$$

$$\frac{P^R}{\Re T}\frac{\mathrm{d}Q^R}{\mathrm{d}x} - 2\pi r^R \sum_i D_i \left.\frac{\mathrm{d}c_i}{\mathrm{d}r}\right|_{r=r^R,x} = 0 \tag{23}$$

These equations represent the partial and total differential mass balances. The first term describes the change of the partial/total molar flux along the reactor length on the retentate side, respectively, while the second term describes the molar flux exchanged between the membrane and the retentate chamber. It was assumed plug flow pattern with negligible total pressure drop and ideal gas behaviour. These assumptions hold also for the permeate side, which mass balance equations are presented below.

The corresponding boundary conditions for Eqs (22)-(23) are as follows (considering tube side feed):

At $x=0$ (tube side inlet), $p_i^R = p_i^F$ and $Q^R = Q^F$ (24)

These equations impose the composition and total volumetric flow rate at the reactor inlet. r^R is the membrane radius for the retentate side ($r^R = r^T$ for tube side feed and $r^R = r^S$ for shell side feed).

MASS BALANCES AND BOUNDARY CONDITIONS FOR THE PERMEATE SIDE

$$\frac{1}{\Re T}\frac{\mathrm{d}\left(Q^P p_i^P\right)}{\mathrm{d}x} + m2\pi r^P D_i \left.\frac{\mathrm{d}c_i}{\mathrm{d}r}\right|_{r=r^P,x} = 0 \tag{25}$$

$$\frac{P^P}{\Re T}\frac{\mathrm{d}Q^P}{\mathrm{d}x} + m2\pi r^P \sum_i D_i \left.\frac{\mathrm{d}c_i}{\mathrm{d}r}\right|_{r=r^P,x} = 0 \tag{26}$$

The corresponding boundary conditions for Eq.s (25)-(26) are as follows (considering tube side feed):

For m=1 (co-current flow), Q^P=0 at x=0 (inlet side)
(27)
For m=-1 (counter-current flow), Q^P=0 at x=L (outlet side) (28)

These equations states that there is no volumetric flow rate at the inlet of the permeate side (no sweeping gas). r^R is the membrane radius for the permeate side (r^P=r^S for tube side feed and r^P=r^T for shell side feed) and L is the length of the tubular membrane. The boundary condition for the partial pressure on the permeate side at x=0 or x=L, according to the type of flow (co-current or counter-current, respectively), is not necessary. As Q^P=0 for such boundary, the term $Q^P p_i^P$ is always zero, independently of the partial pressure value. Anyway, its value can be calculated from the fluxes of each component at the membrane surface (see eq. (29) below).

For cross flow operation mode, the composition of a species on the permeate stream at each axial coordinate is considered to be the ratio between its flux and the total flux of all species that crosses the membrane surface [100], as follows:

$$p_i^P(x) = \frac{D_i \left.\frac{\mathrm{d}c_i}{\mathrm{d}r}\right|_{r=r^P,x}}{\sum_i D_i \left.\frac{\mathrm{d}c_i}{\mathrm{d}r}\right|_{r=r^P,x}} P^P \tag{29}$$

The volumetric flow rate for this arrangement, which is independent of the flow direction, is given by:

$$\frac{P^P}{\Re T}\frac{\mathrm{d}Q^P}{\mathrm{d}x} + 2\pi r^P \sum_i D_i \left.\frac{\mathrm{d}c_i}{\mathrm{d}r}\right|_{r=r^P,x} = 0 \tag{30}$$

Equations (18)-(30) were made dimensionless, becoming as follows:

$$D_i^* \left(\frac{d^2 c_i^*}{d\zeta^2} + \frac{1}{\zeta + r^t/\delta}\frac{dc_i^*}{d\zeta} \right) + \nu_i \Phi^2 f\left(c_i^*\right) = 0 \tag{31}$$

$$f(c_i^*) = \left(c_A^* - c_B^* \frac{\left(C_{ref}\right)^{\Delta n}}{K_e} \right) \tag{32}$$

$$\zeta = j \ \ (\forall\lambda), \ \ c_i^*(\lambda) = S_i^* p_i^{R*}(\lambda) \tag{33}$$

$$\zeta = (1-j) \ \ (\forall\lambda), \ \ c_i^*(\lambda) = S_i^* p_i^{P*}(\lambda) \tag{34}$$

$$\frac{d\left(Q^{R*}p_i^{R*}\right)}{d\lambda}-\left(1+\frac{\delta}{r^t}\right)^j \Gamma D_i^* \left.\frac{dc_i^*}{d\zeta}\right|_{\zeta=j,\lambda}=0 \tag{35}$$

$$P^{R*}\frac{dQ^{R*}}{d\lambda}-\left(1+\frac{\delta}{r^t}\right)^j \Gamma\sum_i D_i^* \left.\frac{dc_i^*}{d\zeta}\right|_{\zeta=j,\lambda}=0 \tag{36}$$

$$\lambda=0,\ p_i^{R*}=p_i^{F*} \quad \text{and} \quad Q^{R*}=1 \tag{37}$$

$$\frac{d\left(Q^{P*}p_i^{P*}\right)}{d\lambda}+m\left(1+\frac{\delta}{r^t}\right)^{1-j} \Gamma D_i^* \left.\frac{dc_i^*}{d\zeta}\right|_{\zeta=1-j,\lambda}=0 \tag{38}$$

$$P^{P*}\frac{dQ^{P*}}{d\lambda}+m\left(1+\frac{\delta}{r^t}\right)^{1-j} \Gamma\sum_i D_i^* \left.\frac{dc_i^*}{d\zeta}\right|_{\zeta=1-j,\lambda}=0 \tag{39}$$

$$m=1:\quad \lambda=0,\quad Q^{P*}=0 \tag{40}$$

$$m=-1:\quad \lambda=1,\quad Q^{P*}=0 \tag{41}$$

$$p_i^{P*}(\lambda)=\frac{D_i^* \left.\frac{dc_i^*}{d\zeta}\right|_{\zeta=1-j,\lambda}}{\sum_i D_i^* \left.\frac{dc_i^*}{d\zeta}\right|_{\zeta=1-j,\lambda}} P^{P*} \tag{42}$$

$$P^{P*}\frac{dQ^{P*}}{d\lambda}+f\left(1+\frac{\delta}{r^t}\right)^{1-j} \Gamma\sum_i D_i^* \left.\frac{dc_i^*}{d\zeta}\right|_{\zeta=1-j,\lambda}=0 \tag{43}$$

where

$$\zeta=(r-r^T)/\delta, \qquad \lambda=x/L,\ \Phi=\delta\left(\frac{k_d\left(C_{ref}\right)^{a-1}}{D_{ref}}\right)^{1/2}, \qquad \Gamma=\frac{2\pi r^T L D_{ref} C_{ref}\Re T}{\delta Q_{ref}P_{ref}}$$

The symbol j defines the configuration feed: j=0 for tube side feed and j=1 for shell side feed. The parameters Φ and Γ were described in the previous model. The remaining symbols are described in the nomenclature section. The numerical details concerning the resolution of this model are described below, in section "*Numerical Methods for Membrane Reactors*".

RESULTS AND DISCUSSION

In the work regarding this model [99, 100, 102], the authors performed several simulations in order to understand how the relative conversion (as defined in the previous model) depended on the different dimensionless parameters and variables. According to the results, the dependence of the reactor conversion with the relative diffusion coefficients, total pressure drop between the upstream and downstream sides and reaction stoichiometry, along the contact time and Thiele modulus parametric space, is basically the same that was described above for the perfectly mixed flow pattern model. They studied further the

influence of the flow configuration (co-current, counter-current and cross flow arrangements), as well as the influence of the feed configuration (through the tube side or through the shell side).

Concerning the flow configuration, it was concluded that the co-current operation mode was the best one, while the counter-current was the worst, being the differences in the reactor performance relevant only for a medium/high dimensionless contact time and for an intermediate range of Thiele modulus values (Figure 7) [100]. For low dimensionless contact times, the net result depends almost exclusively on the retentate composition and flow rate, so the flow configuration has almost no influence. For $\Phi \to \infty$, the chemical reaction tends to be in equilibrium throughout all the membrane thickness, resulting then a limit conversion equal to the thermodynamic equilibrium one.

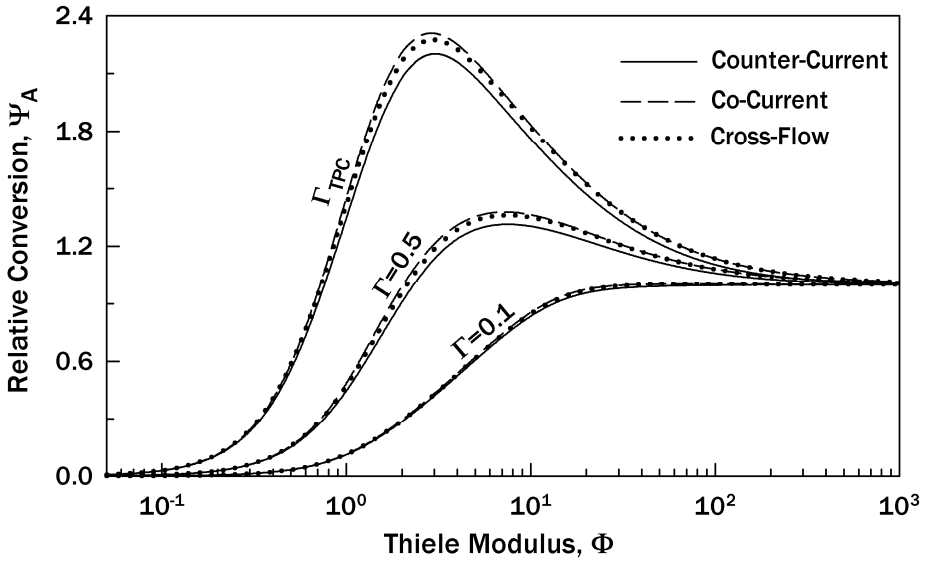

Figure 7. Relative conversion of component A as a function of the Thiele modulus for different flow patterns and dimensionless contact time values. $D_A^* = 1$, $D_B^* = 10$, $S_i^* = 1$, $p_A^{F*} = 1$, $P^{P*} = 0.1$, $r^t/\delta = 10$, $j = 0$ and $R_k = 0.25$. Adapted from [100].

The higher efficiency of the counter-current operating mode when there is only gas separation is the result of a better exploitation of the pressure gradients between the tube and shell sides along the fibre length, as also happens in other processes in chemical engineering (e. g., heat transfer). However, for a catalytic membrane reactor like the one described in this study [100], the partial fluxes through the membrane are not constant. In fact, they depend on the Thiele modulus, on the relative sorption and diffusion coefficients and on the total pressure difference between the upstream and the downstream sides, for a given contact time value [100]. Anyway, the main differences in terms of composition along the reactor length for all flow configurations occurs essentially on the permeate side and for a region of low axial coordinates (inlet reactor region), as it can be realized from Figure 8.

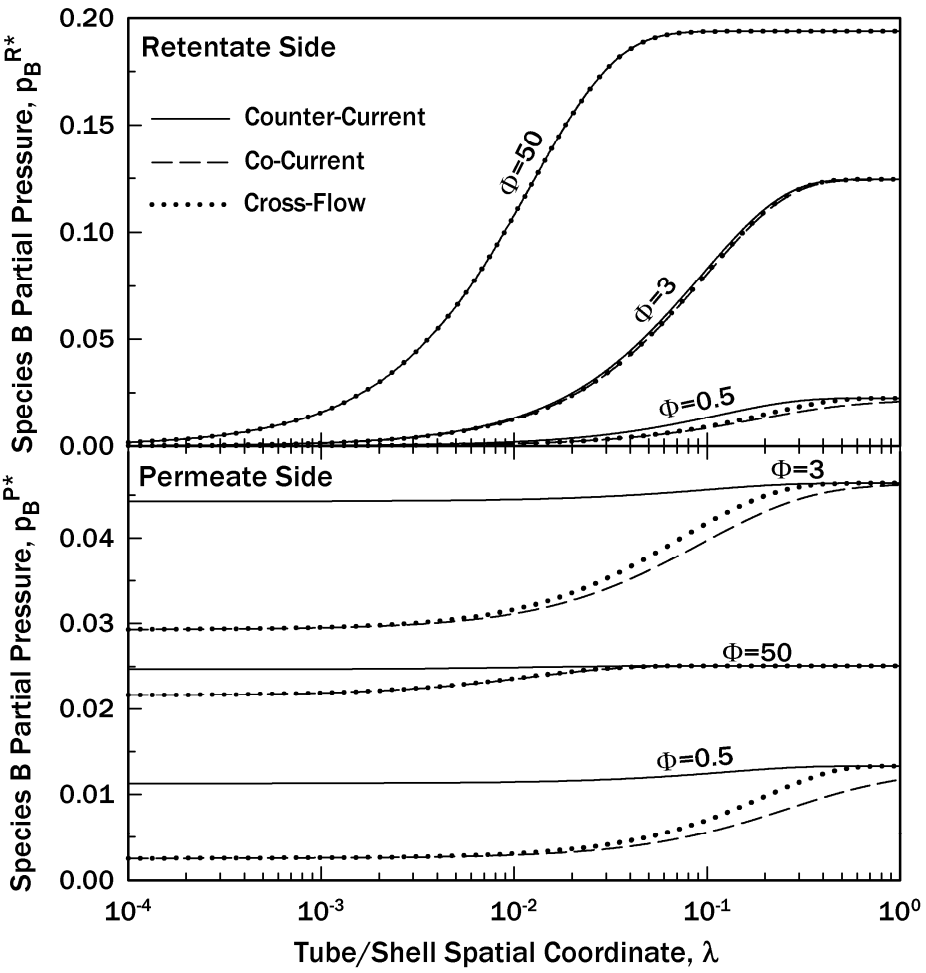

Figure 8. Partial pressure of component B in the retentate (upper part) and permeate (lower part) streams as a function of the axial coordinate, at the TPC and for different Thiele modulus values and flow patterns. Same variable values as in Figure 7. Adapted from [100].

As a consequence, the performance of the reactor depends essentially on what happens in this part of the reactor. Either for co-current or cross flow operating modes, the pressure of component *B* in the permeate stream at this region is the minimum possible (the shell side inlet is closed), maximizing thus the reaction rate inside the membrane (maximum driving force and maximum reactant concentration). For counter-current flow, on the other hand, the concentration of the reaction product for x=0 (exit of the permeate chamber) is higher than for co-current flow, as a result of the production earlier on, that is, for higher axial coordinates. This higher concentration leads to a diffusion of component *B* back to the membrane, as it can be seen in Figure 8 from the slight decreasing of its partial pressure [100].

Relatively to the influence of the reactor feed configuration [100], the simulation results showed that the conversion for a shell side feed was always higher than the one obtained for a tube side feed, for a reaction product permeability higher than the one of the reactant. Figure 9 shows these results for the case of higher reaction product diffusion.

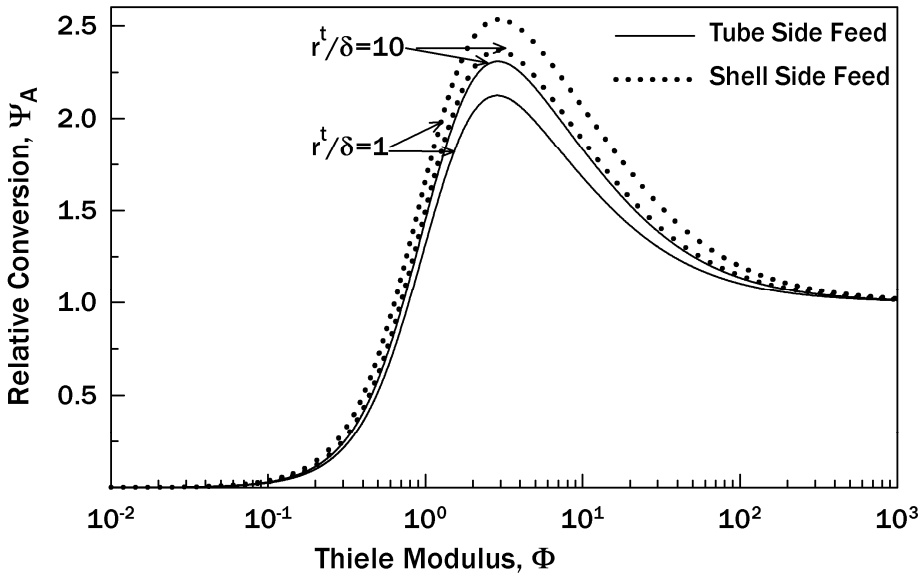

Figure 9. Relative conversion of component A as a function of the Thiele modulus and for different feed locations and r^t/δ ratios. $\Gamma = \Gamma_{TPC}$ and $m = 1$. The other variables have the same values as in Figure 7. Adapted from [100].

The simulation results showed also that the reactor conversion depends on the ratio r^T/δ, as a direct consequence of the cylindrical geometry of the membrane. For high r^T/δ values (membrane approaching the flat shape), the diffusion crossing area is nearly constant as a function of the radial coordinate and the influence of the feed location (tube side or shell side) is negligible (see Figure 10).

As the r^T/δ value decreases (the hollow fibre wall becomes thicker for a given internal radius), the diffusion crossing area as a function of the radius changes more and more, leading to a favourable or unfavourable impact on the concentration of the reaction components. For a tube side feed, the reactant concentration decreases doubly, leading this way to a conversion penalization. This occurs either due to the chemical reaction (consumption of reactant) or due to the membrane cylindrical geometry, which diffusion crossing area increases with the radial coordinate. When the reactor is fed from the shell side, on the other hand, the decreasing of the diffusion crossing area as the reactants proceeds across the membrane thickness lessens the impact of the decreasing of the reactant concentration due to the chemical reaction, enhancing thus the conversion (Figures 9 and 10).

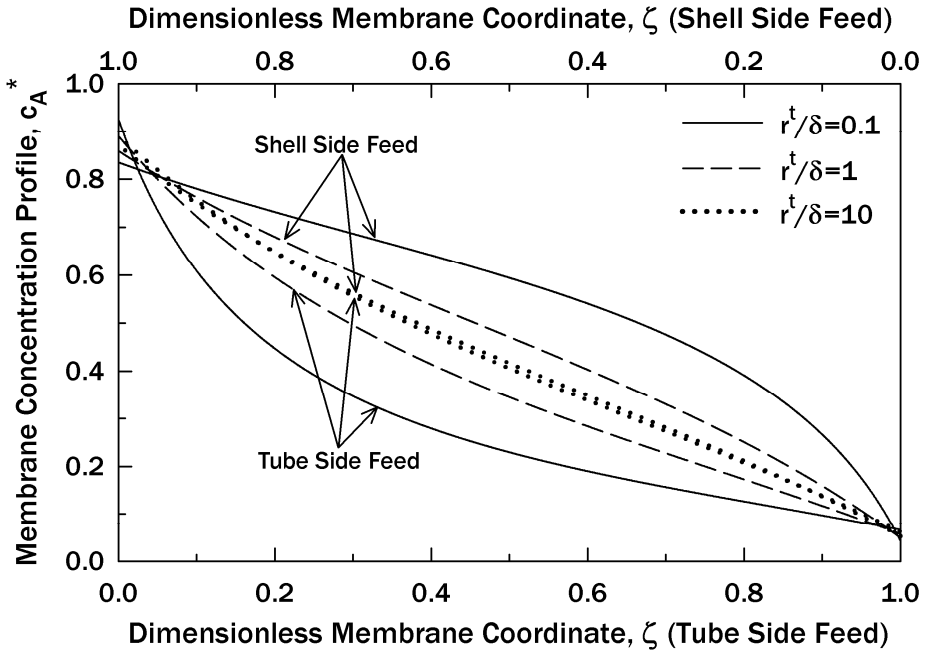

Figure 10. Dimensionless concentration of component A inside the membrane as a function of the radial coordinate for different feed locations and r^t/δ ratios. $\Gamma = \Gamma_{TPC}$, $\Phi = 3$, $\lambda = 1$ and $m = 1$. The other variables have the same values as in Figure 7. Adapted from [102].

For the case where the reaction product permeability is lower than the one of the reactant, the conclusions are different: the best feed location (with respect to the conversion) depends now on the Thiele modulus and contact time values (see Figure 11). For low Thiele modulus, the shell side feed is always better than the tube side feed, whatever is the dimensionless contact time. For medium/high Thiele modulus values, the shell side feed is better than the tube side feed only for low to medium dimensionless contact times. This behaviour is a consequence of two factors: the cylindrical geometry of the membrane, that is, the change of the diffusion crossing area as a function of the membrane radius, and the separation effect [100]. As in the previous case, the influence of the feed location on the conversion becomes irrelevant as the membrane tends to the flat shape.

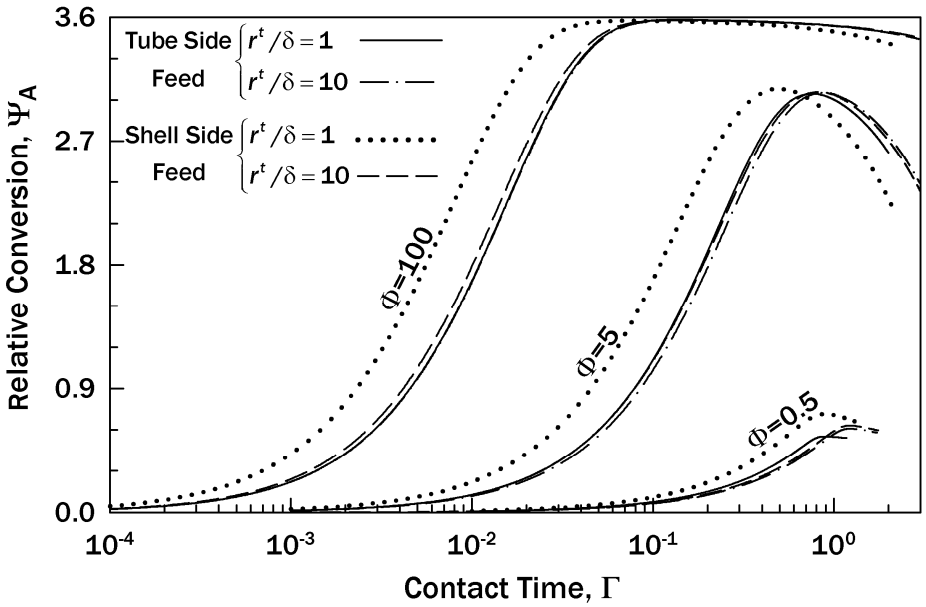

Figure 11. Relative conversion of component A as a function of the contact time for different feed locations, Thiele modulus and r^t/δ ratios. $D_i^* = 1$, $S_A^* = 1$, $S_B^* = 0.1$, $p_A^{F*} = 1$, $P^{P*} = 0.1$, $m = 1$ and $R_k = 0.25$. Adapted from [102].

Nonisothermal/Perfectly-Mixed Flow Pattern Models

More recently, Sousa and Mendes extended the previously developed perfectly mixed flow pattern model to consider now nonisothermal and nonadiabatic conditions [103]. Moreover, the model reaction now considered was much more complex and completely different in nature: a consecutive-parallel reaction describing the hydrogenation $Propyne \rightarrow Propene \rightarrow Propane$. The main objective of such work was to analyze in which conditions a catalytic polymeric membrane could take advantage of its effective diffusivity and sorption selectivities to improve the performance of a PCMR over the one obtained in a conventional reactor for this reaction system. More specifically, the authors tried to answer the question "can the concentration of propyne in the outlet stream be lowered under the levels obtained using a conventional catalytic reactor in a more efficient way"? To answer it, they developed a proper model and performed a set of simulation results to illustrate some key points about the use of such membrane reactor. They performed an analysis of the propyne concentration on the permeate stream along the model parametric space, as well as the possibility of enhancing the selectivity and overall yield to the desirable intermediate product (propene) and the conversion of the main reactants propyne and hydrogen.

DEVELOPMENT OF THE MEMBRANE REACTOR MODEL

The catalytic membrane reactor considered in this study is the same as the one depicted in Figure 1. The reaction studied, the hydrogenation of propyne, was of the consecutive-parallel type:

Reaction 1: $A + B \rightarrow C$ Reaction 2: $B + C \rightarrow D$

with A≡Propyne; B≡Hydrogen; C≡Propene; D≡Propane.

The model proposed for this reactor is based on the same main assumptions as described above, excepting the nonisothermal nature. The corresponding steady-state mass and energy balance equations are described in the following:

MASS BALANCE FOR THE MEMBRANE

$$D_i \frac{d^2 c_i}{dz^2} + \sum_{j=1}^{2} \nu_{ij} k_j(T) f_j(c_i) = 0 \quad (44)$$

where i refers to the i^{th} component, j refers to the j^{th} reaction and ν is the stoichiometric coefficient, taken negative for reactants, positive for reaction products, and null for the components that do not take part in the reaction. $k(T)$ is the reaction rate constant based on the conditions of the reaction medium (in terms of temperature). f is the local reaction rate function, which was given by the following rate expressions:

$$f_1(c_i) = c_A c_B \quad (45)$$

$$f_2(c_i) = c_B \quad (46)$$

The details about the choice of these reaction rate laws are described in [103]. Basically, such a choice was supported in two main points. Firstly, this formulation considerably simplifies the problem, without compromising the main conclusions, although any type of reaction rate expression could be inserted into the catalytic membrane reactor model. Anyway, some published works report that the power-law type rate equations represent the experimental results better than the Langmuir-Hinshelwood-Hougen-Watson models for the same hydrogenation reactions as the one considered in the study now discussed [103]. Secondly, they considered that the reaction rate defined in equation (45) depends on the concentration of reactants propyne and hydrogen, because the concerning concentrations were considered close to each other. For the reaction rate defined in equation (46), on the other hand, they considered zero order relatively to the hydrocarbon (propene), as its concentration was in very large excess relatively to that of hydrogen. So, this reaction was considered of pseudo first order relatively to hydrogen. Concerning the temperature dependence of the reaction rate constants, the authors assumed that they followed an Arrhenius' dependence:

$$k_1(T) = k_1^0 \exp\left(-\frac{E_1}{\Re T}\right) = k_1(T_{ref}) \exp\left[-\frac{E_1}{\Re}\left(\frac{1}{T} - \frac{1}{T_{ref}}\right)\right] \quad (47)$$

$$k_2(T) = k_2^0 \exp\left(-\frac{E_2}{\Re T}\right) = k_2(T_{ref}) \exp\left[-\frac{E_2}{\Re}\left(\frac{1}{T} - \frac{1}{T_{ref}}\right)\right] \quad (48)$$

where k_j^0 and E_j are the pre-exponential reaction rate constant and the activation energy for reaction *j*, respectively.

ENERGY BALANCE FOR THE MEMBRANE

$$\lambda_e \frac{d^2T}{dz^2} + \sum_{i=1}^{4}\left(C_{P,i}(T) D_i \frac{dc_i}{dz}\right)\frac{dT}{dz} + \sum_{j=1}^{2}\left(-\Delta H_j^r\right) k_j(T)\, f_j(c_i) = 0 \quad (49)$$

The first term in this energy balance equation is related to the transport of energy by conduction, while the second term is related with the enthalpy carried by the reaction species. The last term is the energy generation term related to the heat of reaction. In eq. (49), λ_e is the effective thermal conductivity that depends on both thermal conductivities of the solid and sorbed species, ΔH_j^r is the reaction enthalpy for the reaction *j* and $C_{P,i}$ is the heat capacity of species *i* in the sorbed phase.

Following the assumption of negligible external transport limitations at the membrane surface, the boundary conditions for the mass and energy balances are:

At $z=0$ (retentate side), $c_i = S_i p_i^R$ and $T = T^R$ (50)

At $z=\delta$ (permeate side), $c_i = S_i p_i^P$ and $T = T^P$ (51)

PARTIAL AND TOTAL MASS BALANCES FOR THE RETENTATE/PERMEATE SIDES

The partial and total mass balances for the retentate and permeate sides are the same as the ones concerning the model described above (equations 5, 6, 7 and 8), tacking into account, however, the non isothermal conditions.

ENERGY BALANCE FOR THE RETENTATE SIDE

$$\sum_{i=1}^{4}\frac{Q^F p_i^F H_i^F}{\Re T^F}-\sum_{i=1}^{4}\frac{Q^R p_i^R H_i^R}{\Re T^R}+A^m\sum_{i=1}^{4}H_i D_i\left.\frac{dc_i}{dz}\right|_{z=0}+A^m\lambda_e\left.\frac{dT}{dz}\right|_{z=0}+$$
$$A^m\sum_{i=1}^{4}\left(-\Delta H_i^s\right)D_i\left.\frac{dc_i}{dz}\right|_{z=0}-U^{t,R}A^{t,R}\left(T^R-T^{ext}\right)=0 \qquad (52)$$

The first and second terms of equation (52) account for the enthalpy of the gas phase in the feed and retentate streams; the third term accounts for the enthalpy transported by the reaction species that cross the membrane boundaries; the fourth term accounts for the heat exchange by conduction between the bulk gas and the membrane surface; the fifth term accounts for the sorption enthalpy; the last term accounts for the heat transfer between the bulk gas and a heat exchanger where the coolant is at a fixed temperature, T^{ext}. H is the enthalpy for the gas phase and ΔH^S is the sorption enthalpy (that is, the change between the enthalpy of a reaction species in the gas and membrane phases). $U^{t,R}$ and $A^{t,R}$ are the external overall coefficient and external area of heat transfer for the retentate side, respectively.

ENERGY BALANCE FOR THE PERMEATE SIDE

$$\sum_{i=1}^{4}\frac{Q^P p_i^P H_i^P}{\Re T^P}+A^m\sum_{i=1}^{4}H_i D_i\left.\frac{dc_i}{dz}\right|_{z=\delta}+A^m\lambda_e\left.\frac{dT}{dz}\right|_{z=\delta}+$$
$$A^m\sum_{i=1}^{4}\left(-\Delta H_i^s\right)D_i\left.\frac{dc_i}{dz}\right|_{z=\delta}+U^{t,P}A^{t,P}\left(T^P-T^{ext}\right)=0 \qquad (53)$$

The meaning of the different terms in equation (53) is identical to the corresponding ones in equation (52), as well as the hypotheses considered.

DIMENSIONLESS EQUATIONS

The model variables were made dimensionless with respect to the feed conditions (Q^F, P^F and T^F), to component A (D_A, S_A and $C_{P,A}$) and to the membrane thickness, δ. The external and feed temperatures were considered to be equal. The reference temperature was set to 298 K.

In this study, the authors assumed as reasonable to consider a uniform temperature for the catalytic membrane reactor chambers (T^R=T^P), in view of the usually low membrane thickness (few hundred microns, normally) and the perfectly mixed flow pattern assumption for both chambers. According to this hypothesis, the energy balances for the retentate and permeate chambers, equations (52) and (53), respectively, were simplified to a single global energy balance, described by equation (66) below.

Changing for dimensionless variables and introducing suitable dimensionless parameters, the model equations became as follows (the dimensionless mass balance equations for the retentate and permeate chambers are also included here):

$$D_i^* \frac{d^2 c_i^*}{d\zeta^2} + \Phi^2 \sum_{j=1}^{2} \nu_{ij} \kappa_j \left(T^*\right) f_j \left(c_i^*\right) = 0 \tag{54}$$

$$f_1 \left(c_i^*\right) = c_A^* c_B^* \tag{55}$$

$$f_2 \left(c_i^*\right) = c_B^* \tag{56}$$

$$\kappa_1 \left(T^*\right) = \exp\left[\gamma\left(1 - 1/T^*\right)\right] \tag{57}$$

$$\kappa_2 \left(T^*\right) = R_r \exp\left[R_E \gamma\left(1 - 1/T^*\right)\right] \tag{58}$$

$$\frac{1}{Pe_H} \frac{d^2 T^*}{d\zeta^2} + \left(\sum_{i=1}^{4} C_{P,i}^* D_i^* \frac{dc_i^*}{d\zeta}\right) \frac{dT^*}{d\zeta} - \phi^2 \frac{\beta}{Pe_H} \left(\kappa_1 f_1 + R_H \kappa_2 f_2\right) = 0 \tag{59}$$

$$\zeta = 0, \;\; c_i^* = S_i^* p_i^{R*} \text{ and } T^* = T^{R*} \tag{60}$$

$$\zeta = 1, \;\; c_i^* = S_i^* p_i^{P*} \text{ and } T^* = T^{P*} \tag{61}$$

$$\frac{Q^{F*} p_i^{F*}}{T^{F*}} - \frac{Q^{R*} p_i^{R*}}{T^{R*}} + \frac{\Gamma}{\varphi + 1} D_i^* \left.\frac{dc_i^*}{d\zeta}\right|_{\zeta=0} = 0 \tag{62}$$

$$\frac{Q^{F*} P^{F*}}{T^{F*}} - \frac{Q^{R*} P^{R*}}{T^{R*}} + \frac{\Gamma}{\varphi + 1} \sum_{i=1}^{4} D_i^* \left.\frac{dc_i^*}{d\zeta}\right|_{\zeta=0} = 0 \tag{63}$$

$$\frac{Q^{P*} p_i^{P*}}{T^{P*}} + \frac{\Gamma}{\varphi + 1} D_i^* \left.\frac{dc_i^*}{d\zeta}\right|_{\zeta=1} = 0 \tag{64}$$

$$\frac{Q^{P*} P^{P*}}{T^{P*}} + \frac{\Gamma}{\varphi + 1} \sum_{i=1}^{4} D_i^* \left.\frac{dc_i^*}{d\zeta}\right|_{\zeta=1} = 0 \tag{65}$$

$$\begin{aligned} &Q^{F*} \sum_{i=1}^{4} p_i^{F*} C_{P,i}^* - Q^{R*} \sum_{i=1}^{4} p_i^{R*} C_{P,i}^* + \frac{\Gamma}{\varphi + 1} \sum_{i=1}^{4} C_{P,i}^* D_i^* \left.\frac{dc_i^*}{d\zeta}\right|_{\zeta=0} T^{R*} + \\ &\frac{1}{\varphi + 1} \frac{\Gamma}{Pe_H} \left(\left.\frac{dT^*}{d\zeta}\right|_{\zeta=0} - \left.\frac{dT^*}{d\zeta}\right|_{\zeta=1} \right) - St\left(T^{R*} - T^{F*}\right) = 0 \end{aligned} \tag{66}$$

where

$$C_{P,i}^* = C_{P,i}/C_{P,ref}, \qquad T^* = T/T_{ref}, \qquad R_H = \Delta H_2^r/\Delta H_1^r, \qquad R_E = E_2/E_1,$$

$$\Phi = \delta\left[\frac{C_{ref}k_1(T_{ref})}{D_{ref}}\right]^{1/2}, \quad \Gamma = \frac{A^m \Re T_{ref} S_{ref} D_{ref}}{\delta Q_{ref} y_A^F}, \quad St = \frac{U^{t,G} A^{t,G} \Re T_{ref}}{Q_{ref} P_{ref} C_{P,ref}}, \quad \varphi = y_B^F / y_A^F,$$

$$R_r = \frac{1}{C_{ref}} \frac{k_2(T_{ref})}{k_1(T_{ref})}, \quad Pe_H = \frac{C_{ref} C_{P,ref} D_{ref}}{\lambda_e}, \quad \beta = \frac{\Delta H_1^r C_{ref} D_{ref}}{\lambda_e T_{ref}}, \quad \gamma = E_1 / \left(\Re T_{ref}\right)$$

It was assumed that the heat capacity is independent of the pressure/concentration and temperature and that the reference enthalpy is independent of the pressure. Φ is the Thiele modulus, here referred to the first reaction and at the reference temperature; Γ is the dimensionless contact time, now referred to species *A* (reference component); R_r is the ratio of the reaction rate constants at the reference temperature; γ is the Arrhenius' number based on the first reaction; R_H is the ratio of the heats of reaction; R_E is the ratio of the activation energies; Pe_H is the modified heat Peclet number; β is the Prater number based on the first reaction; φ is the ratio between the composition of component *B* and the one of the reference component in the feed stream (referred to the first reaction); *St* is the Stanton number.

The main objective of such work was to determine what improvements could be achieved with a catalytic membrane reactor (CMR) when compared with the more conventional counterpart. "Conventional", in the context of this work, meant a catalytic gas-phase reactor with perfectly mixed flow pattern (CSTR) fed with the same stream and where the same reactions, described by equivalent kinetic equations, took place at the catalyst surface. The performances of these two reactors are not directly comparable. However, the authors assumed that a PCMR with a nonpermselective membrane and operating in the total flow-through configuration (total permeation condition) could be loosely equivalent to such CSTR. This equivalence was discussed in their work and a set of simulations for both reactors, in the above described conditions, showed its validity.

Based on the performed simulations, which numerical procedure is described below, the authors selected the more adequate parametric space in terms of reaction rate (Thiele modulus) and reactor temperature (Stanton number) to reach the goal of their study. The membrane reactor was considered to work at the total permeation condition (the contact time parametric space was not considered as a variable in the study). According to the specifications of the outlet stream in terms of the concentrations of the impurity propyne and the valuable intermediate propene, it would be desirable to maximize the conversion of propyne and minimize the one of propene, that is, maximize the selectivity to the intermediate product, as an industrial typical purified propene stream for the production of polypropylene should contain less than 10 ppm of propadiene and 5 ppm of propyne [103]. Thus, the parametric space of intermediate to high Thiele modulus was selected, to ensure significant reactants conversion. Concerning the Stanton number parameter, an intermediate to high values region was selected, to allow only a moderate temperature rise in the reactor, as an increase in the catalyst temperature has a detrimental effect on the selectivity of the partial hydrogenation product, for the parameters values considered.

The mathematical model regarding this study is described by a large number of parameters and variables. However, most of the parameters values were calculated considering data taken from the literature or were defined according to a qualitative knowledge of the reactions and catalytic membrane considered in the study. In the end, only a few key parameters were considered in this work, namely: the sorption coefficient of

hydrogen, the Thiele modulus and the Stanton number. The membrane considered was a PDMS built-in with nanosized palladium clusters as catalyst. All the sorption and diffusion coefficients for the hydrocarbons were considered to be equal; the diffusion coefficient for hydrogen was considered to be 10 times higher than the one for the hydrocarbons.

The simulated results obtained considering a higher sorption coefficient for hydrogen showed the following main conclusions:

- The propyne conversion reached in the CMR was always enhanced in the entire Thiele modulus/Stanton number parametric space analysed, when compared with the values attained in the equivalent CSTR (ECSTR, Figure 12). However, such an improvement was substantial for the intermediate Thiele modulus region, being only marginal for the medium to high values of the same parameter. Additionally, the conversion of hydrogen attained in the CMR was improved for the lower to medium Thiele modulus values. For the higher Thiele modulus values region, the hydrogen conversion was complete, like what happens in the ECSTR (Figure 12-A).
- The propyne molar fraction in the outlet (permeate) stream was lowered in the same parametric region, especially for the lower values of the Thiele modulus (Figure 12-B).
- Concerning the selectivity and overall yield to the intermediate product, they were considerably penalized in the medium Thiele modulus values region and slightly favoured for higher values (Figures 12-C and 12-D).

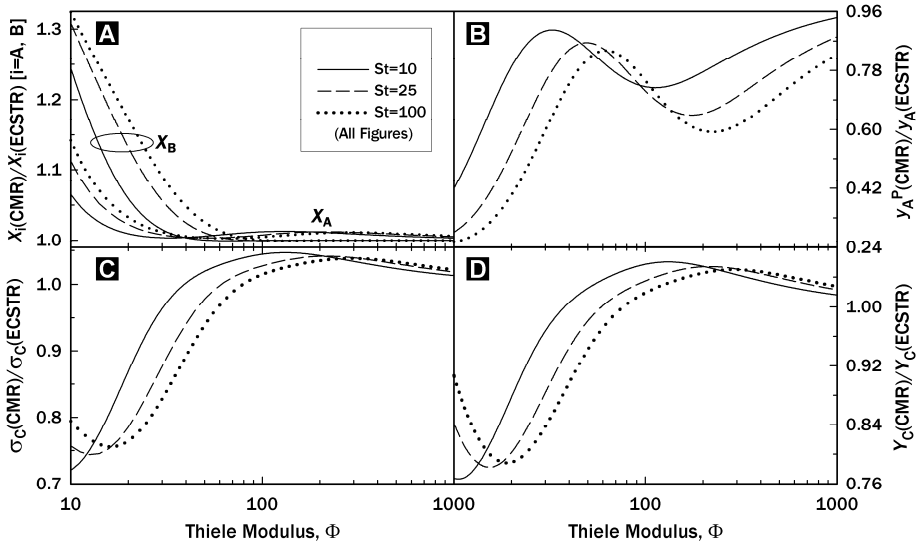

Figure 12: Ratio between the quantities *conversion (X) of propyne and hydrogen* (12-A), *molar fraction (y) of propyne in the permeate stream* (12-B), *selectivity* (σ) *to propene* (12-C) and *overall yield (Y) of propene* (12-D) in the CMR and in the equivalent CSTR, as a function of the Thiele modulus and for different Stanton number values. $D_B^* = 10$, $S_B^* = 10$ and Γ corresponding to the total permeation condition. $Cp_A^* = 1$, $Cp_B^* = 0.469$, $Cp_C^* = 1.054$, $Cp_D^* = 1.214$, $Pe_H = 0.05$, $B = -9.096$, $\gamma = 20$, $\varphi = 1.5$, $R_E = 1.5$, $P^{P*} = 0.5$, $R_r = 0.001$, $R_H = 0.753$, $y_A^F = 0.0465$, $y_B^F = 0.0698$, $y_C^F = 0.8837$. Adapted from [103].

When the sorption coefficient for hydrogen decreases relatively to the one of the hydrocarbons (see Figure 13), the simulation results showed the following main conclusions:

- The propyne conversion attained in the CMR is considerably penalized when compared with the one attained in the equivalent CSTR, especially for the low Thiele modulus values of the parametric space analyzed. However, the difference decreases quickly with an increasing of the Thiele modulus value, disappearing completely for intermediate values of this parameter. The same behaviour is observed for the reactant hydrogen.
- The propyne molar fraction in the outlet (permeate) stream is strongly penalized for the low values of the Thiele modulus parametric space analyzed. As this parameter value increases, such a penalization decreases rapidly and is only marginal for the medium to high values.
- The selectivity to the intermediate product turned to be favoured in the entire region of the Thiele modulus values, especially for the lower ones.
- The overall yield to the intermediate product shows its highest enhancement relatively to the ECSTR for the intermediate Thiele modulus values. As this parameter value increases, the enhancement decreases slowly, tending to disappear for very high values.

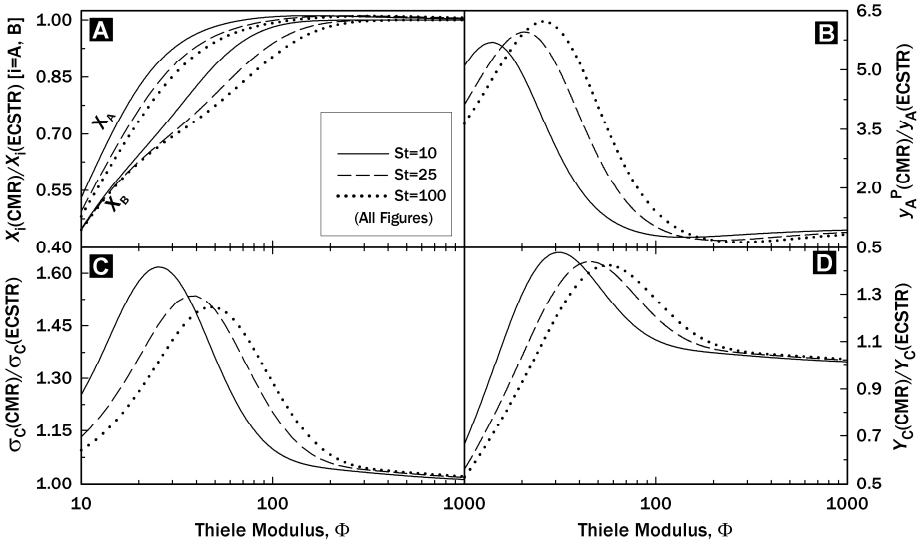

Figure 13: Ratio between the quantities conversion of propyne and hydrogen (13-A), molar fraction of propyne in the permeate stream (13-B), selectivity to propene (13-C) and overall yield of propene (13-D) in the CMR and in the equivalent CSTR, as a function of the Thiele modulus and for different Stanton number values. $D_B^* = 10$, $S_B^* = 0.1$ and Γ corresponding to the total permeation condition. The other parameters are the same as in Figure 12. Adapted from [103].

These results are explained by Sousa and Mendes [103] in terms of the catalytic activity, relative extension of the chemical reactions and relative diffusion and sorption coefficients of the reactant hydrogen.

More recently, Brandão *et al*. [24, 25] also studied the propyne hydrogenation, both theoretically and experimentally. Both the propylene and the consecutive $Propyne \rightarrow Propene \rightarrow Propane$ hydrogenations carried out in a catalytic membrane reactor using a PDMS membrane occluded with nanoclusters of palladium were modelled. The transport parameters of the models were obtained from independent experiments [106] as well as some of the kinetic ones [107, 108]. It was concluded that simulation results compare favourably with the experimental ones obtained at 35 °C.

NUMERICAL METHODS FOR MEMBRANE REACTORS

The previously discussed models by Frisch and co-workers [11, 77], Wu *et al.* [56] and Yawalkar *et al.* [94] constitute a typical boundary value problem with constant boundary conditions. The numerical resolution of such problems is simple and can be performed as follows: the differential equations are discretized, that is, their derivative terms are substituted by numerical approximations at selected positions of the spatial domain (e.g. membrane thickness) – the *discretization grid* –, resulting thus an algebraic system of equations. The solution of such equations system gives the values of the dependent variable (concentration of the reaction components) in the selected spatial points (discretization points).

The space discretization can be carried out by different numerical methods: orthogonal collocation, orthogonal collocation on finite elements, Galerkin finite elements and finite differences. For the resolution of these problems, several numerical packages are available, such as ColNew, for example [109]. MADONNA can also be used to solve such model equations, as it will be shown with some examples presented and discussed in the Appendix section below.

All the available methods to solve the referred steady-state problems need an initial estimate to start the calculations. If the model parameters are such that the concentration profiles inside the membrane are smooth, that is, if the catalytic activity is relatively low, the solution of the model equations is obtained easily and with a good accuracy. However, when the catalytic activity is high, the concentration profiles inside the membrane are steep. In such conditions, a solution with good accuracy demands a discretization grid with a high number of collocation points or finite elements and, even in this case, may be very difficult to obtain, due to problems of convergence.

Considering the above described models [96, 97, 99, 100, 102, 103], the numerical problem becomes more complex (except in the case where an analytical solution for the membrane model equation is available, as mentioned in section "*Isothermal/Plug Flow Pattern Models*"). On one hand, there is a total pressure difference between both sides of the membrane. On the other hand, the boundary conditions are not constant during the calculations. In face of these constraints, we have been using the so-called false transient method to overcome the problems of numerical instability. Basically, this strategy consists in adding a time derivative term to the model equations, more specifically the ones describing the partial mass balances for the retentate and permeate chambers (and the energy equations, for the non-isothermal model), as well as the corresponding ones to the mass (and energy) balances for the membrane. The global mass balance equations for the retentate and permeate chambers can be solved explicitly in order to the volumetric flow rate (perfectly-mixed flow pattern models) [96, 97, 103] or by numerical integration (plug-flow pattern models) [99, 100, 102]. By using a suitable spatial discretization method such as the ones mentioned previously, the partial differential equations (describing the pseudo transient state) are transformed into a set of ordinary differential equations (ODEs). This set of equations can then be solved in the time domain until a steady state solution is obtained, either using simple methods such as Euler (first order convergence) or Runge-Kutta (fourth-fifth order convergence), or using a more sophisticated package such as LSODA [110]. This routine solves initial value problems consisting in stiff or non-stiff systems of first order ODEs, with step size and convergence order both variable. For non-stiff systems, it makes use of the Adams method with a maximum convergence order of 12, while for stiff systems it uses the Gear (or BDF) method with a maximum convergence order of 5. Excepting the isothermal models with analytical solution for the membrane mass balance equation, none of the remaining models presented can be solved using the package MADONNA (the models reporting membrane reactors with variable boundary conditions).

To overcome the problem of using a discretization grid with a high number of collocation points, two different strategies were proposed by our group. In one case [98], it was developed a numerical tool consisting of a wavelet-based algorithm for adapting along the time of integration a non-uniform discretization spatial grid. This strategy proved to be efficient in allocating automatically the necessary density of collocation points along the spatial coordinate, allowing to obtain a solution with high accuracy [98].

Despite the efficiency of this strategy in terms of achieving a solution with high accuracy, it demands a considerable computational effort. In a tentative to simplify the resolution of this kind of problems, an alternative strategy based on a transformation of the independent variable (spatial coordinate) was developed [101]. Basically, this different approach has the same goal as the dynamically adaptive grid described above [98], that is, only a necessary density of collocation points along the spatial domain is used. However, while this task is done dynamically in the wavelet-based algorithm, a constant grid of collocation points along all the integration time is used in this new strategy. Moreover, the discretization grid is defined automatically in the wavelet-based algorithm, while it is more or less empirical in this new strategy, as it implies a previous knowledge about the solution of the problem. This numerical scheme was applied to the solution of some of the developed models using orthogonal collocation for the discretization of the spatial derivative terms and the results obtained were compared with the ones obtained using the wavelet-based method [101], showing to be very efficient to get the solution with high accuracy and with low computational effort.

APPENDIX: EXAMPLES OF APPLICATION USING MADONNA

In this appendix, some examples based on the works presented along the text are solved by the software package MADONNA. This software package solves initial and boundary value problems, so it is not able to solve problems in two or more regions connected through variable boundary conditions. Typically, model equations describing membrane reactors are defined in more than one region. However, there are a few situations where MADONNA can be successful in solving such models. If the membrane model equations have analytical solution, the software can be used to solve the model equations for the retentate and permeate chambers, either as a function of time (for the perfectly-mixed flow pattern) or as a function of the spatial coordinate, that is, along the reactor length (for the plug flow pattern). If the membrane model equations do not have analytical solution, MADONNA can be successful in solving the problem only if the boundary conditions are constant. This situation is valid only for perfectly-mixed flow pattern. The conditions for applicability of MADONNA in this situation are even more restrictive, because the solution is possible only for isothermal regime. In the following, 3 examples are going to be presented in order to illustrate these particular situations.

EXAMPLE 1:

This example is based on the model presented by Kaliaguine and co-workers [56], described in section "*Liquid/Vapour Phase Membrane Reactors*", and shows a situation where the boundary conditions are constant. We should call the reader attention for some small misprints in this reference, concerning the model equations. Anyway, the objective of the presented example is to show how to use the software to solve a specific problem and not to solve a specific model published by anyone. Contrarily to what happen in the original paper [56], the equations of the model presented here are in dimensionless form, because the

numerical errors are minimized, though the reference variables are correctly selected, and the equations become more compact (reduction of the independent variables number). Moreover, the arising of dimensionless groups with physical significance makes the overall analysis of the system easier to perform.

As referred in section "*Liquid/Vapour Phase Membrane Reactors*", this model describes the oxyfunctionalization of *n*-hexane with hydrogen peroxide into a mixture of hexanols and hexanones. The chemical equations considered in this model are the following:

$$C_6H_{14} + H_2O_2 \xrightarrow{k_1} C_6H_{14}O + H_2O \qquad r_1 = \frac{k_1 K_{C_6H_{14}} C_{C_6H_{14}} \left(C_{H_2O_2}\right)^2}{1 + K_{C_6H_{14}} C_{C_6H_{14}} + K_{C_6H_{14}O} C_{C_6H_{14}O}} \quad (67)$$

$$C_6H_{14}O + H_2O_2 \xrightarrow{k_2} C_6H_{12}O + 2H_2O \qquad r_2 = \frac{k_2 K_{C_6H_{14}O} C_{C_6H_{14}O} \left(C_{H_2O_2}\right)^2}{1 + K_{C_6H_{14}} C_{C_6H_{14}} + K_{C_6H_{14}O} C_{C_6H_{14}O}} \quad (68)$$

$$H_2O_2 \xrightarrow{k_3} H_2O + \frac{1}{2}O_2 \qquad r_3 = k_3 \left(C_{H_2O_2}\right)^2 \quad (69)$$

Considering, for simplification, $A \equiv C_6H_{14}$, $B \equiv C_6H_{14}O$ and $C \equiv H_2O_2$, and considering the sorption-diffusion model for the transport through the membrane as assumed by the authors [56], the dimensionless mathematical model equations are as follows:

$$D_A^* \frac{d^2 c_A^*}{d\zeta^2} - \Phi^2 \left[\frac{c_A^* \left(c_C^*\right)^2}{1 + K_A^* c_A^* c_{ref} + K_B^* c_B^* c_{ref}} \right] = 0 \quad (70)$$

$$D_B^* \frac{d^2 c_B^*}{d\zeta^2} - \Phi^2 \left[\frac{k_2}{k_1} \frac{K_B}{K_A} \frac{c_B^* \left(c_C^*\right)^2}{1 + K_A c_A^* c_{ref} + K_B c_B^* c_{ref}} - \frac{c_A^* \left(c_C^*\right)^2}{1 + K_A c_A^* c_{ref} + K_B c_B^* c_{ref}} \right] = 0 \quad (71)$$

$$D_C^* \frac{d^2 c_C^*}{d\zeta^2} - \Phi^2 \left[\frac{c_A^* \left(c_C^*\right)^2}{1 + K_A c_A^* c_{ref} + K_B c_B^* c_{ref}} + \frac{k_2}{k_1} \frac{K_B}{K_A} \frac{c_B^* \left(c_C^*\right)^2}{1 + K_A c_A^* c_{ref} + K_B c_B^* c_{ref}} + \frac{k_3}{k_1} \frac{1}{K_A} \frac{\left(c_C^*\right)^2}{c_{ref}} \right] = 0 \quad (72)$$

The corresponding boundary conditions are as follows:

At $\zeta = 0$, $c_A^* = 0$, $c_B^* = 0$, $c_C^* = 0.159$ (73)

At $\zeta = 1$, $c_A^* = 1.00$, $c_B^* = 0$, $c_C^* = 0$ (74)

These boundary conditions describe an interfacial reactor where each of the reactants (*A* and *C*) is fed to the different sides of the membrane and is immiscible in the other phase, as well as the immiscibility of the main reaction product (*B*) in both aqueous and organic phases. The dimensionless variables (referred with an "*" in superscript) are defined in the same way

as the equations presented in section "*Gas Phase Membrane Reactors*". Species *A* (*n*-hexane) was chosen to be the reference component, hence $D_{ref} = 2.56 \times 10^{-7}\ \mathrm{m^2\ h^{-1}}$. The reference concentration was considered the one of the reference component at the membrane surface, hence $c_{ref} = 5.11\ \mathrm{kmol\ m^{-3}}$. k_i is the kinetic constant for reaction *i* and K_i is the equilibrium constant of adsorption for component *i*. Φ is the Thiele modulus $\left(\Phi = \delta c_{ref} \sqrt{\frac{\rho_b k_1 K_A}{D_{ref}}} \right)$, where $\rho_b \left(\mathrm{kg\ m^{-3}} \right)$ is the density of the catalyst in the catalytic membrane. The other variables have the usual meaning and are defined in the nomenclature section. Table 4 contains the values considered for the different variables in the simulations according to the authors [56].

Table 4. Nondimensionless variables values used in the simulations

Reaction Components	C_6H_{14}	$C_6H_{14}O$	H_2O_2
Surface concentration at z=0 (kmol m^{-3})	0	0	0.81
Surface concentration at z=δ (kmol m^{-3})	5.11	0	0
Equilibrium adsorption constants (m^3 $kmol^{-1}$)	19.3	0.21	––
Diffusion coefficients (m^2 h^{-1})	$2.56x10^{-7}$	$1.33x10^{-7}$	$1.12x10^{-8}$
Kinetic constants (m^6 $kmol^{-1}$ kg^{-1} h^{-1})	$k_1=8.60x10^{-3}$	$k_2=1.75x10^{-2}$	$k_3=2.90x10^{-3}$

The authors [56] analysed the influence of the membrane thickness (δ) for the different values given in the paper, as well as the respective diffusivities. However, the membrane thickness is incorporated in the Thiele modulus parameter in the present example. So, the reader can analyse which is the influence of that variable in the respective concentration profiles of the reaction species inside the membrane by performing the simulations for different Thiele modulus values. Relatively to the density of the catalyst (ρ_b), the authors do not say anything about. However, despite this variable appears only in the Thiele modulus parameter, we should call the reader's attention that its influence in real systems embraces the kinetic parameter, as well as the diffusion coefficients of the reaction components. Figure 14 shows the dimensionless concentration profiles across the catalytic membrane thickness for Φ=25 and Table 5 contains the values from the simulations. These results were obtained using the software MADONNA with a step size of 0.001 and a tolerance of $1x10^{-8}$. The concerning code for example 1 is presented in the following:

```
METHOD RK4
{ Run this example through Model -> Modules -> Boundary Value ODE

Set as Boundary Conditions:
CA(1)=1
CB(1)=0
CC(1)=0

Set as Unknowns:
```

```
INIT CA'; Min=0.5; Max=1.5
INIT CB'; Min=-0.1; Max=0.1
INIT CC'; Min=-1; Max=0

Set Tolerance=1E-8 }

STARTTIME = 0
STOPTIME= 1
DT = 0.001
DTOUT=0.1

RENAME TIME= r

{Model parameters}
thiele=25.
CRef=5.11
DRef=2.56E-7

{Diffusion coefficients}
DA=2.56E-7/DRef
DB=1.33E-7/DRef
DC=1.12E-8/DRef
{Kinetic constants}
k1=8.6E-3
k2=1.75E-2
k3=2.9E-3

{Equilibium constants}
KA=19.3
KB=0.21

{Initial conditions}
INIT CA = 0
INIT CA' = 1
INIT CB = 0
INIT CB' = 0.1
INIT CC = 0.81/CRef
INIT CC' = -1

{Component A}
FA=CA*CC^2/(1+KA*CA*CRef+KB*CB*CRef)
CA'' = thiele^2*FA/DA

{Component B}
FB1=CA*CC^2/(1+KA*CA*CRef+KB*CB*CRef)
FB2=CB*CC^2/(1+KA*CA*CRef+KB*CB*CRef)
```

```
FB=-FB1+k2/k1*KB/KA*FB2
CB'' = thiele^2*FB/DB

{Component C}
FC=FB1+k2/k1*KB/KA*FB2+k3/k1*1/KA*1/CRef*CC^2
CC'' = thiele^2*FC/DC
```

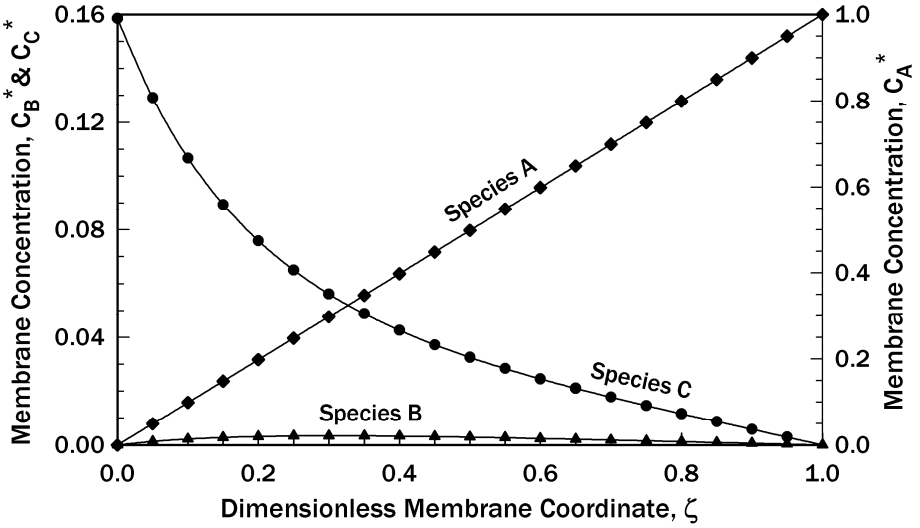

Figure 14. Dimensionless concentration of reaction components inside the membrane as a function of the dimensionless spatial coordinate. The values of the variables used in the simulations are referred in the text.

Table 5. Dimensionless concentration values of the reaction components along the membrane thickness (although the results were obtained using a step size of 0.001, the table shows only a few points for simplicity)

ζ	c_A^*	c_B^*	c_C^*
0.0	0	0	0.15851
0.1	0.09885	0.00221	0.10670
0.2	0.19837	0.00314	0.07585
0.3	0.29824	0.00339	0.05615
0.4	0.39831	0.00325	0.04258
0.5	0.49850	0.00289	0.03256
0.6	0.59875	0.00241	0.02460
0.7	0.69904	0.00184	0.01782
0.8	0.79936	0.00124	0.01168
0.9	0.89968	0.00062	0.00580
1.0	1	0	0

EXAMPLE 2:

This example is based on the model presented above in section "*Isothermal/Perfectly-Mixed Flow Pattern Models*" [98]. It considers perfectly-mixed flow pattern and a chemical reaction of the type $A \rightleftarrows B$, for which there is an analytical solution for the diffusion-reaction equations across the membrane thickness. The model equations to be solved by the package MADONNA comprehend the unsteady-state ODEs that result from the mass balances for the retentate and permeate chambers, as follows:

$$\frac{dp_i^{R*}}{d\theta} = Q^{F*} p_i^{F*} - Q^{R*} p_i^{R*} + \Gamma D_i^* \left.\frac{dc_i^*}{d\zeta}\right|_{\zeta=0} \tag{75}$$

$$\frac{dp_i^{P*}}{d\theta} = \left[Q^{P*} p_i^{P*} + \Gamma D_i^* \left.\frac{dc_i^*}{d\zeta}\right|_{\zeta=1} \right] \frac{\tau^R}{\tau^P} \tag{76}$$

These equations were obtained from equations (5) and (7) by including the transient term. $\theta = \frac{t}{\tau^R}$ is the dimensionless time based on the retentate conditions. $\tau^R = \frac{V^R}{Q_{ref}}$ and $\tau^P = \frac{V^P}{Q_{ref}}$ are the residence times for the retentate and permeate chambers, respectively, where *V* means the chamber volume. The other symbols have already been described above and are referred in the nomenclature section. The reference variables and conditions are the same as the ones described in section "*Isothermal/Perfectly-Mixed Flow Pattern Models*". We should call the reader's attention for the fact that the membrane process was considered to be in pseudo steady state, that is, the residence time for the membrane is much less than the residence time for the retentate and permeate chambers. If this assumption is not considered, the mass balance for the membrane should be written in addition to equations (75) and (76), considering the necessary relation between all the residence times.

The corresponding initial conditions, defined as pure reactant *A* in both retentate and permeate chambers at the respective dimensionless total pressures, are as follows:

$$\text{At } \theta = 0,\ p_A^{R*} = 1,\ p_B^{R*} = 0,\ p_A^{P*} = 0.01,\ p_B^{P*} = 0 \tag{77}$$

The dimensionless retentate and permeate volumetric flow rates are calculated from the global mass balance equations (eqs. (14) and (16)), described in the following (remember that the retentate and permeate total pressures are constant, so $\sum \frac{dp_i^{R*}}{d\theta} = \sum \frac{dp_i^{P*}}{d\theta} = 0$ and $\sum p_i^{F*} = \sum p_i^{R*} = 1$, equations (75) and (76) above):

$$Q^{R*} = 1 + \Gamma \sum_i D_i^* \left.\frac{dc_i^*}{d\zeta}\right|_{\zeta=0} \tag{78}$$

$$Q^{P*} = -\frac{\Gamma \sum_i D_i^* \left. \frac{dc_i^*}{d\zeta} \right|_{\zeta=1}}{P^{P*}} \tag{79}$$

The derivative terms of the flux at the membrane surfaces are described by the following analytical equations [98], considering the reference variables and conditions described in section "*Isothermal/Perfectly-Mixed Flow Pattern Models*":

$$\left. \frac{dc_A^*}{d\zeta} \right|_{\zeta=0} = J_2 + J_3\psi - J_4\psi \tag{80}$$

$$\left. \frac{dc_A^*}{d\zeta} \right|_{\zeta=1} = J_2 + J_3\psi\, exp(\psi) - J_4\psi\, exp(-\psi) \tag{81}$$

$$\left. \frac{dc_B^*}{d\zeta} \right|_{\zeta=0} = J_2 K_e - \frac{J_3\psi}{D_B^*} + \frac{J_4\psi}{D_B^*} \tag{82}$$

$$\left. \frac{dc_B^*}{d\zeta} \right|_{\zeta=1} = J_2 K_e - \frac{J_3\psi\, exp(\psi)}{D_B^*} + \frac{J_4\psi\, exp(-\psi)}{D_B^*} \tag{83}$$

where

$$\psi = \Phi\left(1 + \frac{1}{D_B^* K_e}\right)^{1/2} \qquad \Phi = \delta\left(\frac{k_d}{D_{ref}}\right)^{1/2}, \qquad J_1 = \frac{p_A^{R*} + D_B^* S_B^* p_B^{R*}}{1 + K_e D_B^*},$$

$$J_2 = \frac{\left(p_A^{P*} + D_B^* S_B^* p_B^{P*}\right) - \left(p_A^{R*} + D_B^* S_B^* p_B^{R*}\right)}{1 + K_e D_B^*},$$

$$J_3 = \frac{D_B^*\, exp(-\psi)\left[exp(-\psi)\left(K_e p_A^{R*} - S_B^* p_B^{R*}\right) - K_e p_A^{P*} + S_B^* p_B^{P*}\right]}{\left(1 + K_e D_B^*\right)\left(exp(-2\psi) - 1\right)},$$

$$J_4 = \frac{-D_B^*\left[K_e p_A^{R*} - S_B^* p_B^{R*} - exp(-\psi)\left(K_e p_A^{P*} - S_B^* p_B^{P*}\right)\right]}{\left(1 + K_e D_B^*\right)\left(exp(-2\psi) - 1\right)}$$

At this point, we should call the reader's attention for the following: after a threshold Thiele modulus value, the term $exp(\psi)$ in equations (81) and (83) takes values too high and an overflow error appears during the calculations. However, the term $J_3.exp(\psi)$ can be simplified adequately ($exp(\psi)exp(-\psi)=1$), avoiding such a possible overflow error.

The values of the variables and parameters considered in the simulations are presented in Table 6. Figure 15 shows the dimensionless partial pressure of the reaction components as a function of time (retentate and permeate chambers) and Table 7 contains the respective values. These results were obtained with MADONNA using a step size of $1x10^{-5}$.

The concerning code for example 2 is presented in the following:

```
METHOD RK4

STARTTIME = 0
STOPTIME= 0.22
DT = 0.00001
DTOUT=0.02

{Parameters}
THIELE=4
TAU=0.50538
TAUR=1
TAUP=1

{Feed composition}
PAF=1
PBF=0

{Dimensionless total pressures}
PP=0.01
PR=1

{Dimensionless diffusion coefficients}
DA=1
DB=10

{Dimensionless sorption coefficients}
SA=1
SB=1

{Equilibrium constant}
Ke=0.25

{Initial conditions}
INIT PAR = 1.0
INIT PBR = 0.0
INIT PAP = 0.01
INIT PBP = 0.0

PSI=THIELE*(1+1/(DB*Ke))^0.5

J1=(PAR+DB*SB*PBR)/(1+Ke*DB)
J2=((PAP+DB*SB*PBP)-(PAR+DB*SB*PBR))/(1+Ke*DB)
J3=DB*EXP(-PSI)*(EXP(-PSI)*(Ke*PAR-SB*PBR)-
Ke*PAP+SB*PBP)/((1+Ke*DB)*(EXP(-2*PSI)-1))
J4=-DB*(Ke*PAR-SB*PBR-EXP(-PSI)*(Ke*PAP-SB*PBP))/((1+Ke*DB)*(EXP(-
2*PSI)-1))
```

```
DCADR0=J2+J3*PSI-J4*PSI
DCADR1=J2+J3*PSI*EXP(PSI)-J4*PSI*EXP(-PSI)
DCBDR0=J2*Ke/SB-J3*PSI/(DB*SB)+J4*PSI/(DB*SB)
DCBDR1=J2*Ke/SB-J3*PSI*EXP(PSI)/(DB*SB)+J4*PSI*EXP(-PSI)/(DB*SB)

QR=(1+TAU*(DA*SA*DCADR0+DB*SB*DCBDR0))/(PR)
QP=-TAU*(DA*SA*DCADR1+DB*SB*DCBDR1)/(PP)

{Component A in retentate chamber}
PAR' = PAF-QR*PAR+TAU*DA*DCADR0

{Component B in retentate chamber}
PBR' = PBF-QR*PBR+TAU*DB*DCBDR0

{Component A in permeate chamber}
PAP' = (-QP*PAP-TAU*DA*DCADR1)*TAUR/TAUP

{Component B in permeate chamber}
PBP' = (-QP*PBP-TAU*DB*DCBDR1)*TAUR/TAUP
```

Table 6. Dimensionless variables and parameters values used in the simulations

	Component A	**Component B**	
D_i^*	1	10	
S_i^*	1	1	
p_i^{F*}	1	0	
Φ			4
Γ			0.50538*
K_e			0.25
P^{R*}			1
P^{P*}			0.01
τ^R/τ^P			1

* This value for the contact time parameter corresponds to the total permeation condition.

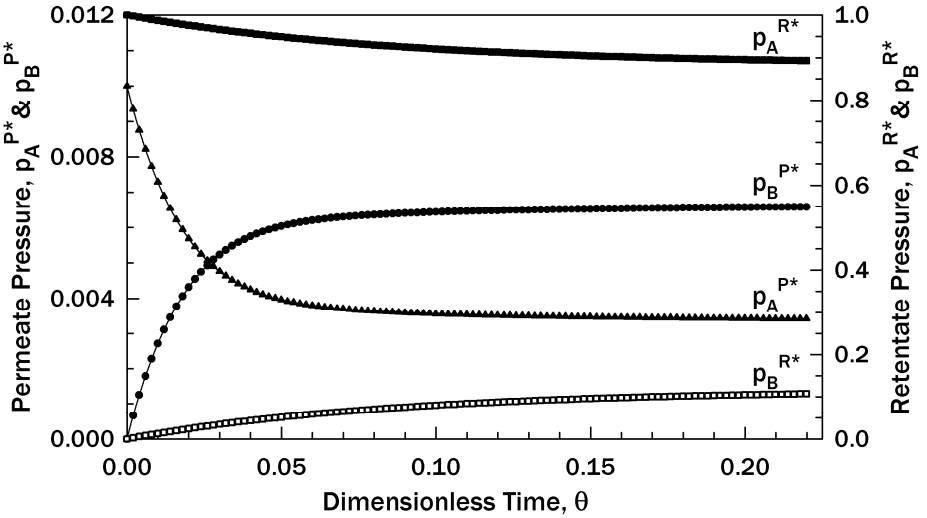

Figure 15. Dimensionless retentate and permeate pressure of reaction components along the dimensionless time. The values of the variables used in the simulations are referred in the text.

Table 7. Dimensionless pressure values of the reaction components along the dimensionless time

θ	p_A^{R*}	p_B^{R*}	p_A^{P*}	p_B^{P*}
0.000000	1.000000	0.000000	0.010000	0.000000
0.020004	0.975867	0.024133	0.005681	0.004319
0.040009	0.956770	0.043230	0.004249	0.005751
0.060013	0.941681	0.058319	0.003800	0.006200
0.080017	0.929748	0.070252	0.003640	0.006360
0.100021	0.920296	0.079704	0.003563	0.006437
0.120026	0.912798	0.087202	0.003516	0.006484
0.140030	0.906843	0.093157	0.003484	0.006516
0.160034	0.902108	0.097892	0.003460	0.006540
0.180038	0.898340	0.101660	0.003442	0.006558
0.200043	0.895339	0.104661	0.003428	0.006572
0.220047	0.892949	0.107051	0.003417	0.006583

EXAMPLE 3:

This example is based on the model presented and discussed above in section "*Isothermal/Plug Flow Pattern Models*" [99, 100]. It considers plug flow pattern with constant pressure on the retentate and permeate chambers and a chemical reaction of the type $A \rightleftarrows B$, for which there is an analytical solution for the diffusion-reaction equations through the membrane, as referred in the previous example. The model equations to be solved

by the package MADONNA comprehend in this case the steady-state ODEs that result from the mass balances for the retentate and permeate chambers. We should call the reader's attention for the fact that the equations presented in the following apply for a flat membrane, contrarily to what was presented in [99, 100] and discussed in the section "*Isothermal/Plug Flow Pattern Models*", namely equations (35)-(40). The reason is because the analytical solution in cylindrical coordinates implies the calculation of Bessel functions, which are not available in MADONNA and can not be easily implemented in the software package, contrarily to the exponential functions. Anyway, a tubular membrane with an internal radius much higher than its thickness can be considered as a flat membrane. For more details, see [99, 100].

Considering then these assumptions, the respective mass balance equations are as follows:

$$\frac{d\left(Q^{R*} p_i^{R*}\right)}{d\lambda} - \Gamma D_i^* \left.\frac{dc_i^*}{d\zeta}\right|_{\zeta=0,\,\lambda} = 0 \tag{84}$$

$$P^{R*} \frac{dQ^{R*}}{d\lambda} - \Gamma \sum_i D_i^* \left.\frac{dc_i^*}{d\zeta}\right|_{\zeta=0,\,\lambda} = 0 \tag{85}$$

$$\frac{d\left(Q^{P*} p_i^{P*}\right)}{d\lambda} + \Gamma D_i^* \left.\frac{dc_i^*}{d\zeta}\right|_{\zeta=1,\,\lambda} = 0 \tag{86}$$

$$P^{P*} \frac{dQ^{P*}}{d\lambda} + \Gamma \sum_i D_i^* \left.\frac{dc_i^*}{d\zeta}\right|_{\zeta=1,\,\lambda} = 0 \tag{87}$$

The boundary conditions for the retentate and permeate side are defined by setting the composition and total volumetric flow rate at the reactor inlet region (λ=0). For the retentate side, the concerning values are the ones of the feed stream:

$$\lambda = 0,\ p_i^{R*} = p_i^{F*} \quad \text{and} \quad Q^{R*} = 1 \tag{88}$$

For the permeate side, the volumetric flow rate is zero (no sweeping gas):

$$\lambda = 0,\quad Q^{P*} = 0 \tag{89}$$

For numerical reasons, the initial condition used in the calculations performed by MADONNA in this example is $1x10^{-9}$. Concerning the composition for λ=0, it can be calculated through equation (42), presented in the following:

$$p_i^{P*}(0) = \frac{D_i^* dc_i^*/d\zeta\big|_{\zeta=1,\,0}}{\sum_i D_i^* dc_i^*/d\zeta\big|_{\zeta=1,\,0}} P^{P*} \tag{90}$$

This equation states that the molar fraction of each reaction component at the beginning of the permeate side is equal to the ratio between its flux and the total flux. The partial pressures are obtained by multiplying the respective molar fractions by the total permeate pressure.

The calculation of $p_i^{P*}(0)$ from equation (90) is not a straightforward task, because the derivative terms $dc_i^*/d\zeta\big|_{\zeta=1,\,0}$ are themselves functions of the boundary conditions. However, substituting the derivative terms in equation (90) by the respective functions described in example 2, namely equations (81) and (83), and making the correct simplifications by using the boundary conditions, a quadratic equation in p_A^{P*} is obtained:

$$A\left(p_A^{P*}\right)^2 + Bp_A^{P*} - C = 0 \qquad (91)$$

with

$$A = \left(1 - D_B^* S_B^*\right)\left(1 + K_e D_B^*\right),$$

$$B = \left\{\left(D_B^* S_B^* P^{P*} - 1\right)\left(1 + K_e D_B^*\right) - P^{P*}\left(1 - D_B^* S_B^*\right) + \psi D_B^* P^{P*}\left(K_e + S_B^*\right)\frac{exp(-2\psi) + 1}{\left(exp(-2\psi) - 1\right)}\right\} \text{ and}$$

$$C = \left\{D_B^* S_B^* P^{P*} - 1 + \psi D_B^* \frac{2K_e\, exp(-\psi) + S_B^* P^{P*}\left(exp(-2\psi) + 1\right)}{\left(exp(-2\psi) - 1\right)}\right\} P^{P*}$$

The solution of equation (91) is obtained by taking the negative part of the square root term. It is not easy to realize from the analysis of such equation which is the correct solution. However, performing previously some calculations considering the values for the variables, it becomes evident which solution is the correct one. If the permeability of component *B* is 1 (that is, $D_B^* S_B^* = 1$), equation (91) becomes linear and the solution is straightforward.

All the previous symbols have already been described above and are referred in the nomenclature section.

The values of the variables and parameters considered in the simulations are presented in Table 8. Figures 16 and 17 show the concentration profiles for the dimensionless partial pressure of the reaction components and volumetric flow rates along the reactor length (retentate and permeate sides), respectively. Tables 9 and 10 contain the respective values, which were obtained with MADONNA using a step size of $1x10^{-5}$. The concerning code for example 3 is presented in the following:

```
METHOD RK4

STARTTIME = 0
STOPTIME= 1
DT = 0.00001
DTOUT=0.1
```

```
RENAME TIME=LAMBDA

{Parameters}
THIELE=10
TAU=0.1

{Dimensionless total pressures}
PP=0.1
PR=1

{Dimensionless diffusion coefficients}
DA=1
DB=5

{Dimensionless sorption coefficients}
SA=1
SB=1

{Equilibrium constant}
Ke=0.25

{Dimensionless parameter}
PSI=THIELE*(1+1/(DB*Ke))^0.5

{Initial pressure in the permeate chamber}
a = (1-DB*SB)*(1+Ke*DB)
b = (DB*SB*PP-1)*(1+Ke*DB)-PP*(1-DB*SB)+PSI*DB*PP*(Ke+SB)*(EXP(-2*PSI)+1)/(EXP(-2*PSI)-1)
c = -(DB*SB*PP-1+PSI*DB*(2*Ke*EXP(-PSI)+SB*PP*(EXP(-2*PSI)+1))/(EXP(-2*PSI)-1))*PP
PAP0 = (-b -SQRT(b^2-4*a*c))/(2*a)
PBP0 = PP-PAP0

{Initial conditions}
INIT PAR = 1.0
INIT PBR = 0.0
INIT QR  = 1.0
INIT PAP = PAP0
INIT PBP = PBP0
INIT QP  = 1e-9 {The initial condition QP=0 cannot be used otherwise a division by 0 would occur}

J1=(PAR+DB*SB*PBR)/(1+Ke*DB)
J2=((PAP+DB*SB*PBP)-(PAR+DB*SB*PBR))/(1+Ke*DB)
J3=DB*EXP(-PSI)*(EXP(-PSI)*(Ke*PAR-SB*PBR)-Ke*PAP+SB*PBP)/((1+Ke*DB)*(EXP(-2*PSI)-1))
```

J4=-DB*(Ke*PAR-SB*PBR-EXP(-PSI)*(Ke*PAP-SB*PBP))/((1+Ke*DB)*(EXP(-2*PSI)-1))

DCADR0=J2+J3*PSI-J4*PSI
DCADR1=J2+J3*PSI*EXP(PSI)-J4*PSI*EXP(-PSI)
DCBDR0=J2*Ke/SB-J3*PSI/(DB*SB)+J4*PSI/(DB*SB)
DCBDR1=J2*Ke/SB-J3*PSI*EXP(PSI)/(DB*SB)+J4*PSI*EXP(-PSI)/(DB*SB)

{Component A in retentate chamber}
PAR' = 1/QR*(TAU*DA*DCADR0-PAR/PR*TAU*(DA*DCADR0+DB*DCBDR0))
{Component B in retentate chamber}
PBR' = 1/QR*(TAU*DB*DCBDR0-PBR/PR*TAU*(DA*DCADR0+DB*DCBDR0))

{Retentate flow rate}
QR' = 1/PR*TAU*(DA*DCADR0+DB*DCBDR0)

{Component A in permeate chamber}
PAP' = -1/QP*(TAU*DA*DCADR1-PAP/PP*TAU*(DA*DCADR1+DB*DCBDR1))

{Component B in permeate chamber}
PBP' = -1/QP*(TAU*DB*DCBDR1-PBP/PP*TAU*(DA*DCADR1+DB*DCBDR1))

{Permeate flow rate}
QP' = -1/PP*TAU*(DA*DCADR1+DB*DCBDR1)

Table 8. Dimensionless variables and parameters values used in the simulations

	Component A	**Component B**	
D_i^*	1	5	
S_i^*	1	1	
p_i^{F*}	1	0	
Φ			10
Γ			0.1
K_e			0.25
P^{R*}			1
P^{P*}			0.1

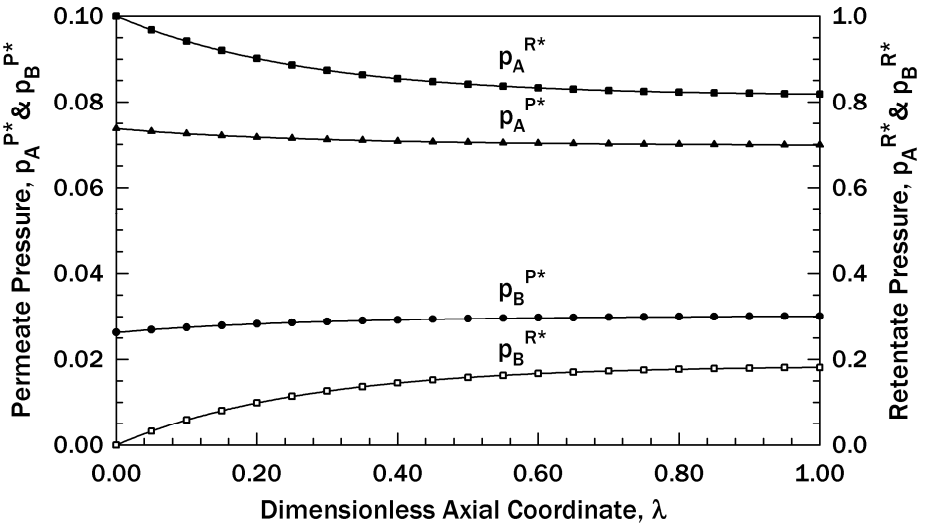

Figure 16. Dimensionless retentate and permeate pressure of reaction components along the tube and shell sides. The values of the variables used in the simulations are referred in the text.

Table 9. Dimensionless pressure values of the reaction components along the reactor length

λ	p_A^{R*}	p_B^{R*}	p_A^{P*}	p_B^{P*}
0	1	0	0.0737493	0.0262507
0.1	0.941587	0.0584131	0.0725272	0.0274728
0.2	0.901457	0.0985432	0.0717176	0.0282824
0.3	0.873868	0.126132	0.0711621	0.0288379
0.4	0.854926	0.145074	0.0707719	0.0292281
0.5	0.841957	0.158043	0.0704934	0.0295066
0.6	0.833113	0.166887	0.0702922	0.0297078
0.7	0.82711	0.17289	0.0701455	0.0298545
0.8	0.823057	0.176943	0.0700378	0.0299622
0.9	0.820338	0.179662	0.0699583	0.0300417
1	0.818524	0.181476	0.0698992	0.0301008

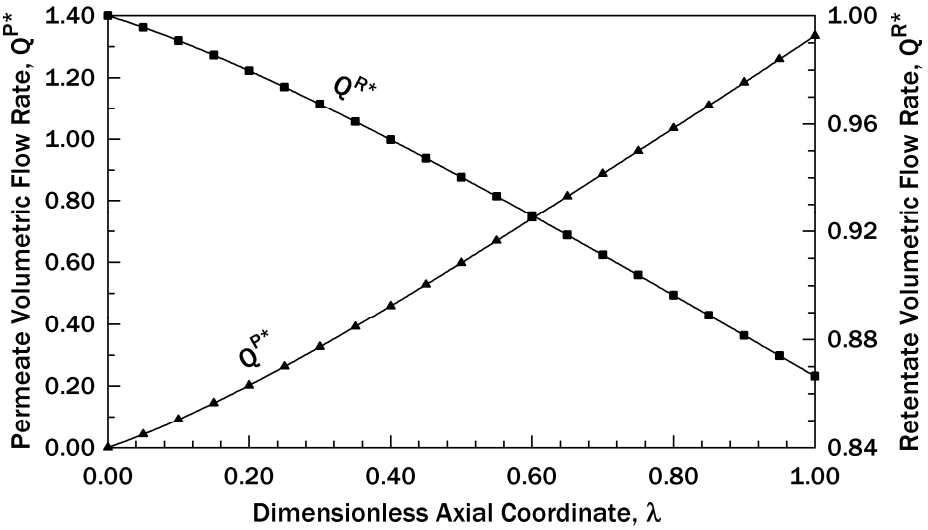

Figure 17. Dimensionless retentate and permeate volumetric flow rates along the tube and shell sides. The values of the variables used in the simulations are referred in the text.

Table 10. Dimensionless volumetric flow rates along the reactor length

λ	Q^{R*}	Q^{P*}
0	1	1.00E-09
0.1	0.990835	0.0916517
0.2	0.979762	0.202381
0.3	0.967377	0.32623
0.4	0.954091	0.459091
0.5	0.940187	0.598129
0.6	0.925862	0.741383
0.7	0.91125	0.887502
0.8	0.896444	1.03556
0.9	0.881509	1.18491
1	0.866486	1.33514

NOMENCLATURE

A External area. [m^2]
B Adiabatic temperature rise. [-]
c Partial intramembrane concentration. [mol m^{-3}]
C Total intramembrane concentration. [mol m^{-3}]
C_P Heat capacity. [J mol^{-1} K^{-1})]
D Diffusion coefficient. [m^2 s^{-1}]
Da Damköhler number. [-]

E Activation energy. [J mol^{-1}]
H Enthalpy. [J mol^{-1}]
k_d Direct reaction rate constant (reversible reactions). [$(mol\ m^{-3})^{1-a-b}\ s^{-1}$]
K_e Thermodynamic equilibrium constant based on feed conditions. [$(mol\ m^{-3})^{c+d-a-b}$]
k_j^0 Pre-Exponential reaction rate constant for the reaction j (irreversible reactions). [$(m^3\ mol^{-1})^{2-j}\ s^{-1}$]
k_j Reaction rate constant for the reaction j (irreversible reactions). [$(m^3\ mol^{-1})^{2-j}\ s^{-1}$]
Pe_H Modified heat Peclet number. [-]
P Total pressure. [Pa]
p Partial pressure. [Pa]
Q Volumetric flow rate. [$m^3\ s^{-1}$]
r Spatial radial coordinate perpendicular to the membrane surface. [m]
$\Re$ Universal gas constant. [J $mol^{-1}\ K^{-1}$)]
R_E Ratio of the activation energies. [-]
R_H Ratio of the heat of reaction. [-]
R_k Ratio between the direct an reverse reaction rate constants. [$(mol\ m^{-3})^{c+d-a-b}$]
R_r Ratio of the reaction rate constants. [-]
S Henry's sorption coefficient. [mol $m^{-3}\ Pa^{-1}$)]
St Stanton number. [-]
T Absolute temperature. [K]
U Heat transfer coefficient. [J $m^{-2}\ s^{-1}\ K^{-1}$]
x Tube/Shell spatial coordinate. [m]
X Conversion. [-]
y Molar fraction. [-]
Y_C Overall yield to species C. [-]
z Membrane spatial coordinate. [m]

Greek symbols

β Prater number based on reaction 1. [-]
γ Arrhenius' number based on reaction 1. [-]
Γ Dimensionless contact time based on species A. [-]
δ Membrane thickness. [m]
ζ Dimensionless membrane spatial coordinate. [-]
θ Dimensionless time. [-]
Θ Relative reaction coefficient. [-]
κ Dimensionless reaction rate constant. [-]
λ Dimensionless tube/shell spatial coordinate. [-]
λ_e Effective thermal conductivity. [J $m^{-1}\ s^{-1}\ K^{-1}$]
ν Stoichiometric coefficient. [-]

($\nu_{A,1}=-1,\ \nu_{B,1}=-1,\ \nu_{C,1}=1,\ \nu_{D,1}=0,\ \nu_{A,2}=0,\ \nu_{B,2}=-1,\ \nu_{C,2}=-1,\ \nu_{D,2}=1$). [-]

σ_C Selectivity to species *C*. [-]

τ Residence time. [s]

φ Ratio of the reactants composition in the feed stream (based on reaction 1). [-]

Φ Thiele modulus. [-]

Ψ_A Relative conversion (ratio between the conversion of reactant A, X_A, and the thermodynamic equilibrium one based on the feed conditions, X_A^E) [-]

Ω Dimensionless heat generation parameter. [-]

Subscripts

i Component *i*. [-]

j Reaction *j*. [-]

ref Reference conditions or component. [-]

Superscripts

* Dimensionless variable. [-]

F Relative to the feed stream conditions. [-]

G Relative to the entire reactor (*Stanton* number definition). [-]

m Relative to the membrane. [-]

O Relative to the exit conditions (CSTR model equations). [-]

P Relative to the permeate chamber conditions. [-]

r Relative to reaction. [-]

R Relative to the retentate chamber conditions. [-]

s Relative to the sorbed phase. [-]

REFERENCES

[1] Ozdemir, S. S., Buonomenna, M. G., Drioli, E. (2006). Catalytic polymeric membranes: Preparation and application. *Appl. Catal. A: Gen*, 307, 167.

[2] Koros, W. J., Chern, R. T. (1987). *Separation of gaseous mixtures using polymer membranes*. in: Ronald W. Rousseau (Ed.). Handbook of separation process technology, John Wiley and Sons, pp. 862-953.

[3] Lütz, S., Rao, N. N.,Wandrey, C. (2006). Membranes in biotechnology (review). *Chem. Eng. Technol*, 29, 1404.

[4] Seen, A. J. (2001). Nafion: An excellent support for metal-complex catalysts. *J. Mol. Catal. A: Chem*, 177, 105.

[5] Vankelecom, I. F. J. (2002). Polymeric membranes in catalytic reactors. *Chem. Rev*, 102, 3779.

[6] Koros, W. J., Woods, D. G. (2001). Elevated temperature application of polymer hollow-fiber membranes. *J. Membr. Sci,* 181, 157.

[7] Rezac, M. E., Schöberl, B. (1999). Transport and thermal properties of poly(ether imide)/acetylene-terminated monomer blends. *J. Membr. Sci*, 156, 211.

[8] Vankelecom, I. F. J., Vercruysse, K. A. L., Neys, P. E., Tas, D. W. A., Janssen, K. B. M., Knops-Gerrits, P. P., Jacobs, P. A. (1998). Novel catalytic membranes for selective reactions. *Topics Catal*, 5, 125.

[9] Song, I. K., Lee, W. Y. (2003). Heteropolyacid (HPA)-polymer composite films as heterogeneous catalysts and catalytic membranes. *Appl. Catal. A: Gen*, 256, 77.

[10] Vankelecom, I. F. J., Scheppes, E., Hus, R., Uytterhoeven, J. B. (1994). Parameters influencing zeolite incorporation in PDMS membranes. *J. Phys. Chem*, 98, 12390.

[11] Frisch, H. L., Maaref, S., Deng-Nemer, H. (1999). Low-temperature dehydrogenation reaction-separation membrane using zeolite 13 X polyethylacrylate. *J. Membr. Sci*, 154, 33.

[12] Rezac, M. E., Koros, W. J., Miller, S. J. (1994). Membrane-assisted dehydrogenation of n-butane. Influence of membrane properties on system performance. *J. Membr. Sci*, 93, 193.

[13] Gryaznov, V. M., Mischenko, A. P., Smirnov, V. S., Aladyshev, S. I. (1973). *Catalytic reactor designed for carrying out conjugate chemical reactions*. US Patent 3,779,711.

[14] Gao, H., Xu, Y., Liao, S., Liu, R., Yu, D. (1993). Catalytic hydrogenation and gas permeation properties of metal-containing poly(phenylene oxide) and polysulfone. *J. Appl. Polym. Sci*, 50, 1035.

[15] Gao, H., Xu, Y., Liao, S., Liu, R., Liu, J., Li, D., Yu, D., Zhao, Y., Fan, Y. (1995). Catalytic polymeric hollow-fiber reactors for the selective hydrogenation of conjugated dienes. *J. Membr. Sci,* 106, 213.

[16] Yu, Z., Xu, Y., Liao, S., Liu, R. (1996). Catalytic behaviors and gas permeation properties of palladium-containing phenophthalein poly(ether sulfone). *J. Appl. Polym. Sci*, 61, 599.

[17] Liu, C., Xu, Y., Liao, S., Yu, D., Zhao, Y., Fan, Y. (1997). Selective hydrogenation of propadiene and propyne in propene with catalytic polymeric hollow-fiber reactor. *J. Membr. Sci*, 137, 139.

[18] Liu, C., Xu, Y., Liao, S., Yu, D. (1998). Mono- and bimetallic catalytic hollow-fiber reactors for the selective hydrogenation of butadiene in 1-butene. *Appl. Catal. A: Gen*, 172, 23.

[19] Liu, C., Xu, Y., Liao, S., Yu, D. (2000). Selective hydrogenation of cyclopentadiene in mono- and bimetallic catalytic hollow-fiber reactors. *J. Mol. Catal. A: Chem*, 157, 253.

[20] Ciebien, J. F., Cohen, R. E., Duran, A. (1998). Catalytic properties of palladium nanoclusters synthesized within diblock copolymer films: hydrogenation of ethylene and propylene. *Supramol. Sci*, 5, 31.

[21] Ciebien, J. F., Cohen, R. E., Duran, A. (1999). Membrane catalysts for partial hydrogenation of 1,3-butadiene: catalytic properties of palladium nanoclusters synthesized within diblock copolymer films. *Mater. Sci. Eng*. C 7, 45.

[22] Theis, J., Fritsch, D., Keil, F. (1997).*Catalysis with nonporous membranes loaded with nanoscale metallic clusters*. in: Proceedings of the ESF, Network Catalytic Membrane Reactors-Final Workshop: Applications and Future Possibilities of Catalytic Membrane Reactors, Turnhout, Belgium, October 16-17, pp. 35-41.

[23] Ziegler, S., Theis, J., Fritsch, D. (2001). Palladium modified porous polymeric membranes and their performance in selective hydrogenation of propyne. *J. Membr. Sci*, 187, 71.

[24] Brandão, L., Fritsch, D., Mendes, A. M., Madeira, L. M. (2007). Propylene

hydrogenation in a continuous polymeric catalytic membrane reactor. *Ind. Eng. Chem. Res*, 46, 5278.

[25] Brandão, L., Madeira, L. M., Mendes, A. M. (2007). Propyne hydrogenation in a continuous polymeric catalytic membrane reactor. *Chem. Eng. Sci*, 62, 6768.

[26] Schmidt, A., Haidar, R., Schomäcker, R. (2005). Selectivity of partial hydrogenation reactions performed in a pore-through-flow catalytic membrane reactor. *Catal. Today*, 104, 305.

[27] Fritsch, D., Bengtson, G. (2006). Development of catalytic reactive porous membranes for the selective hydrogenation of sunflower oil. *Catal. Today*, 118, 121.

[28] Ilinitch, O. M., Simonov, P. A., Cuperus, F. P. (1998). Nanosize palladium loaded catalytic membrane: preparation and cis-trans selectivity in hydrogenation of sunflower oil. *Stud. Surf. Sci. Catal*, 118, 55.

[29] Bottino, A., Capannelli, G., Comite, A., Di Felice, R. (2002). Polymeric and ceramic membranes in three-phase catalytic membrane reactors for the hydrogenation of methylenecyclohexane. *Desalination*, 144, 411.

[30] Byun, H., Lee, T. (2002). Hydrogenation of cyclohexene with perfluorinated cation- and anion-exchange membranes supported platinum. *Desalination*, 144, 419.

[31] Bengtson, G., Scheel, H., Theis, J., Fritsch, D. (2002). Catalytic membrane reactor to simultaneously concentrate and react organics. *Chem. Eng. J*, 85, 303.

[32] Bengtson, G., Oehring, M., Fritsch, D. (2004). Improved dense catalytically active polymer membranes of different configuration to separate and react organics simultaneously by pervaporation.*Chem. Eng. Process*, 43, 1159.

[33] Bengtson, G., Panek, D., Fritsch, D. (2007). Hydrogenation of acetophenone in a pervaporative catalytic membrane reactor with online mass spectrometric monitoring. *J. Membr. Sci*, 293, 29.

[34] Lüdtke, K., Peinemann, K. V., Kasche, V., Behling, R. D. (1998). Nitrate removal of drinking water by means of catalytically active membranes. *J. Membr. Sci*, 151, 3.

[35] Ilinitch, O. M., Gribov, E. N., Simonov, P. A. (2003). Water denitrification over catalytic membranes: hydrogen spillover and catalytic activity of macroporous membranes loaded with Pd and Cu. *Catal. Today*, 82, 49.

[36] Fritsch, D., Kuhr, K., Mackenzie, K., Kopinke, F. D. (2003). Hydrodechlorination of chloroorganic compounds in ground water by palladium catalysts Part 1. Development of polymer-based catalysts and membrane reactor tests. *Catal. Today*, 82, 105.

[37] Bellobono, I. R., Barni, B., Gianturco, F. (1995). Pre-industrial experience in advanced oxidation and integral photodegradation of organics in potable waters and waste waters by PHOTOPERM™ membranes immobilizing titanium dioxide and promoting photocatalysts. *J. Membr. Sci*, 102, 139.

[38] Gianturco, F., Vianelli, L., Tatti, L., Rota, F., Bruzzi, P., Rivas, L., Bellobono, I. R., Bianchi, M., Muntau, H. (1996). Pilot-plant photomineralization of dichloromethane and tetrachloroethene in aqueous solution, by photocatalytic membranes immobilizing titanium dioxide and photopromoters. *Chemosphere*, 33, 1531.

[39] Barni, B., Cavicchioli, A., Riva, E., Zanoni, L., Bignoli, F., Bellobono, I. R., Giantureo, F., De Giorgi, A., Muntau, H., Montanarella, L., Facchetti, S., Castellano, L. (1995). Pilot-plant-scale photodegradation of phenol in aqueous solution by photocatalytic membranes immobilizing titanium dioxide (PHOTOPERM® Process). *Chemosphere*, 30, 1861.

[40] Tatti, L., Niego, D., Rota, F., Bruzzi, P., Moroni, A., Bellobono, I. R., Bonardi, M., Bianchi, M., Muntau, H. (1997). Mathematical modelling of pilot-plant photomineralization of chlorophenols in aqueous solution, by photocatalytic membranes immobilizing titanium dioxide. *Chemosphere*, 34, 41.

[41] Rivas, L., Bellobono, I. R., Ascari, F. (1997). Photomineralization of n-alkanoic acids in aqueous solution by photocatalytic membranes. Influence of trialkyl vanadates as catalytic promoters of immobilized titanium dioxide. *Chemosphere*, 35, 2899.

[42] Morris, R. E., Krikanova, E., Shadman, F. (2004). Photocatalytic membrane for removal of organic contaminants during ultra-purification of water. *Clean Techn. Environ*, Policy 6, 96.

[43] Molinari, R., Pirillo, F., Loddo, V., Palmisano, L. (2006). Heterogeneous photocatalytic degradation of pharmaceuticals in water by using polycrystalline TiO_2 and a nanofiltration membrane reactor.*Catal. Today*, 118, 205.

[44] Lopez, A., Kiwi, J. (2001). Modeling the performance of an innovative membrane-based reactor. Abatement of azo dye (Orange II) up to biocompatibility. *Ind. Eng. Chem. Res*, 40, 1852.

[45] Fontananova, E., Donato, L., Drioli, E., Lopez, L. C., Favia, P., d'Agostino, R. (2006). Heterogenization of polyoxometalates on the surface of plasma-modified polymeric membranes. *Chem. Mater*, 18, 1561.

[46] Pozzo, R. L., Baltanás, M. A., Cassano, A. E. (1997). Supported titanium oxide as photocatalyst in water decontamination: State of the art. *Catal. Today*, 39, 219.

[47] Bellobono, I. R. (1989). Sensitisation and stabilization of organometallic compounds acting as photocatalysts and photosensitisers in photochemical radical polymerization process. *European Patent*, 421512.

[48] Parton, R. F., Vankelecom, I. F. J., Casselman, M. J. A., Bezoukhanova, C. P., Uytterhoeven, J. B., Jacobs, P. A. (1994). An efficient mimic of cytochrome P-450 from a zeolite-encaged iron complex in a polymer membrane. *Nature*, 370, 541.

[49] Langhendries, G., Baron, G. V., Vankelecom, I. F. J., Parton, R. F., Jacobs, P. A. (2000). Selective hydrocarbon oxidation using a liquid-phase catalytic membrane reactor. *Catal. Today*, 56, 131.

[50] Parton, R. F., Vankelecom, I. F. J., Tas, D., Janssen, K. B. M., Knops-Gerrits, P.P., Jacobs, P. A. (1996). Membrane occluded catalysts: A higher order mimic with improved performance. *J. Mol. Catal. A: Chem*, 113, 283.

[51] Vankelecom, I. F. J., Parton, R. F., Casselman, M. J. A., Uytterhoeven, J. B., Jacobs, P. A. (1996). Oxidation of cyclohexane using FePcY-zeozymes occluded in polydimethylsiloxane membranes. *J. Catal*, 163, 457.

[52] Knops-Gerrits, P. P., Vankelecom, I. F. J., Béatse, E., Jacobs, P. A. (1996). Epoxidation of olefines with PDMS membranes containing zeolite occluded manganese diimine complexes. *Catal. Today*, 32, 63.

[53] Neys, P. E. F., Severeyns, A., Vankelecom, I. F. J., Ceulemans, E., Dehaen, W., Jacobs, P. A. (1999). Manganese porphyrins incorporated in PDMS: selective catalysts for the epoxidation of deactivated alkenes. *J. Mol. Catal. A: Chem*, 144, 373.

[54] Neys, P. E. F., Vankelecom, I. F. J., L'abbe, M., Parton, R. F., Cenlemans, E., Dehaen, W., L'abbe, G., Jacobs, P. A. (1998). Manganese- and iron-porphyrins embedded in a polydimethylsiloxane membrane: a selective oxidation catalyst. *J. Mol. Catal. A: Chem*, 134, 209.

[55] Wu, S. Q., Bouchard, C., Kaliaguine, S. (1998). Zeolite containing catalytic membranes as interphase contactors. *Res. Chem. Intermed*, 24, 273.

[56] Wu, S., Gallot, J. E., Bousmina, M., Bouchard, C., Kaliaguine, S. (2000). Zeolite containing catalytic membranes as interphase contactors. *Catal. Today*, 56, 113.

[57] Kaliaguine, S., Bouchard, C., Wu, S. Q., Shu, J. (1998). Use of catalytic membranes as interphase contactors for multiphase reactions. *Canadian Patent*, 2206626.

[58] Lee, J. K., Song, I. K., Lee, W. Y., Kim, J. J. (1996). Modification of 12-molybdophosphoric acid catalyst by blending with polysulfone and its catalytic activity for 2-propanol conversion reaction. *J. Mol. Catal. A: Chem*, 104, 311.

[59] Lee, J. K., Song, I. K., Lee, W. Y. (1997). Design of novel catalyst imbedding heteropoly acids in polymer films: Catalytic activity for ethanol conversion. *J. Mol. Catal. A: Chem*, 120, 207.

[60] Espro, C., Frusteri, F., Arena, F., Parmaliana, A. (2000). Selective oxidation of propane on a Nafion-based catalytic membrane mediated by Fe^{II}-H_2O_2 Fenton system. *J. Mol. Catal. A: Chem*, 159, 359.

[61] Espro, C., Arena, F., Frusteri, F., Parmaliana, A. (2001). On the potential of the multifunctional three phase catalytic membrane reactor in the selective oxidation of light alkanes by Fe^{2+}-H_2O_2 Fenton system. *Catal. Today*, 67, 247.

[62] Espro, C., Frusteri, F., Arena, F., Parmaliana, A. (2003). Innovative membrane-based catalytic process for environmentally friendly synthesis of oxygenates. *Topics Catal*, 22, 65.

[63] Espro, C., Bonura, G., Arena, F., Frusteri, F., Parmaliana, A., Sini, F., Solinas, V. (2004). Factors affecting the efficiency of Nafion-based catalytic membranes in the selective oxidation of light paraffins mediated by the Fenton system. *Catal. Today*, 91-92, 215.

[64] Espro, C., Arena, F., Tasselli, F., Regina, A., Drioli, E., Parmaliana, A. (2006). Selective oxidation of propane on Nafion/PEEK-WC catalytic membranes in a multifunctional reaction system. *Catal. Today*, 118, 253.

[65] Frusteri, F., Arena, F., Bellitto, S., Parmaliana, A. (1999). Partial oxidation of light paraffins on supported superacid catalytic membranes. *Appl. Catal. A: Gen*, 180, 325.

[66] Frusteri, F., Espro, C., Arena, F., Passalacqua, E., Patti, A., Parmaliana, A. (2000). Partial oxidation of propane on Nafion supported catalytic membranes. *Catal. Today*, 61, 37.

[67] Ilinitch, O. M., Vetchinova, Y. S. (1995). Membrane assisted liquid phase catalytic oxidation of sulfides. *Catal. Today*, 25, 423.

[68] Solovieva, A. B., Belkina, N. V.,Vorobiev, A. V. (1996). Catalytic process of alcohol oxidation with target product pervaporation. *J. Membr. Sci*, 110, 253.

[69] Buonomenna, M. G., Lopez, L. C., Barbieri, G., Favia, P., d'Agostino, R., Drioli, E. (2007). Sodium tungstate immobilized on plasma-treated PVDF membranes: New efficient heterogeneous catalyst for oxidation of secondary amines to nitrones. *J. Mol. Catal. A: Chem*, 273, 32.

[70] Molinari, R., Poerio, T., Argurio, P. (2006). One-step production of phenol by selective oxidation of benzene in a biphasic system. *Catal. Today*, 118, 52.

[71] von Landon, G., Moll, J. D., Plowman, K. R., McIntyre, J. A. (1998). Reactor and method for synthesis of hydrogen peroxide. *World Patent*, WO9802379.

[72] Castanheiro, J. E., Fonseca, I. M., Ramos, A. M., Oliveira, R., Vital, J. (2005).

Hydration of α-pinene over molybdophosphoric acid immobilized in hydrophobically modified PVA membranes. *Catal. Today*, 104, 296.

[73] Castanheiro, J. E., Ramos, A. M., Fonseca, I., Vital, J. (2003). The acid catalysed reaction of α-pinene over molybdophosphoric acid immobilised in dense polymeric membranes. *Catal. Today,* 82, 187.

[74] Vital, J., Ramos, A. M., Silva, I. F., Valente, H., Castanheiro, J. E. (2000). Hydration of α-pinene over zeolites and activated carbons dispersed in polymeric membranes. *Catal. Today*, 56, 167.

[75] Vital, J., Ramos, A. M., Silva, I. F., Valente, H., Castanheiro, J. E. (2001). The effect of α-terpineol on the hydration of α-pinene over zeolites dispersed in polymeric membranes. *Catal. Today*, 67, 217.

[76] Feldman, J., Orchin, M. (1990). Membrane-supported rhodium hydroformylation catalysts. *J. Mol. Catal*, 63, 213.

[77] Frisch, H. L., Huang, L., Zeng, W. (2000). Low-temperature cis to trans isomerization reaction-separation membrane using zeolite 13X polyethylacrylate. *J. Membr. Sci*, 170, 35.

[78] Castanheiro, J. E., Ramos, A. M., Fonseca, I. M., Vital, J. (2006). Esterification of acetic acid by isoamylic alcohol over catalytic membranes of poly(vinyl alcohol) containing sulfonic acid groups. *Appl. Catal. A: Gen*, 311, 17.

[79] Liu, Q., Jia, P., Chen, H. (1999). Study on catalytic membranes of $H_3PW_{12}O_{40}$ entrapped in PVA. *J. Membr. Sci,* 159, 233.

[80] Zhu, Y., Chen, H. (1998). Pervaporation separation and pervaporation-esterification coupling using cross-linked PVA composite catalytic membranes on porous ceramic plate. *J. Membr. Sci*, 138, 123.

[81] Fritsch, D., Randjelovic, I., Keil, F. (2004). Application of a forced-flow catalytic membrane reactor for the dimerisation of isobutene. *Catal. Today*, 98, 295.

[82] Randjelovic, I., Bengtson, G., Fritsch, D. (2002). Catalytic membranes: alkene dimerisation by means of acidic porous thin-film composite membranes. *Desalination*, 144, 417.

[83] Choi, J. S., Song, I. K., Lee, W. Y. (2001). Performance of shell and tube-type membrane reactors equipped with heteropolyacid-polymer composite catalytic membranes. *Catal. Today*, 67, 237.

[84] Lee, J. K., Song, I. K., Lee, W. Y. (1994). Methyl tert-butyl ether decomposition over heteropoly acid catalyst in a cellulose acetate membrane reactor. *Catal. Lett*, 29, 241.

[85] Ho, W. S. (2003). CO_2-selective membrane process and system for reforming a fuel to hydrogen for a fuel cell. *US Patent*, 6, 579, 331.

[86] Joong, K., Baoan, L., Hägg, M. (2004). Novel fixed-site-carrier polyvinylamine membrane for carbon dioxide capture. *Journal of Polymer Science, B: Polymer Physics*, 42, 4326.

[87] Hägg, M., Joong, K., Baoan, L. (2007). Membrane for separating CO_2 and process for the production thereof. EP1740291.

[88] Huang, J., El-Azzami, L., Ho, W. S. W. (2005). Modeling of CO_2-selective water gas shift membrane reactor for fuel cell. *J. Membr. Sci,* 261, 67.

[89] Grainger, D., Hägg, M. (2008). Techno-economic evaluation of a PVAm CO_2-selective membrane in an IGCC power plant with CO_2 capture. *Fuel,* 87, 14.

[90] Zou, J., Huang, J., Ho, W. S. W. (2007). CO_2-selective water gas shift membrane reactor for fuel cell hydrogen processing. *Ind. Eng. Chem. Res*, 46, 2272.
[91] Fritsch, D., Peinemann, K. V. (1995). Catalysis with homogeneous membranes loaded with nanoscale metallic clusters and their preparation. *Catal. Today*, 25, 277.
[92] Guerreiro, L., Castanheiro, J. E., Fonseca, I. M., Martin-Aranda, R. M., Ramos, A. M., Vital, J. (2006). Transesterification of soybean oil over sulfonic acid functionalised polymeric membranes. *Catal. Today*, 118, 166.
[93] Wijmans, J. G., Baker, R. W. (1995). The solution-diffusion model: a review. *J. Membr. Sci*, 107, 1.
[94] Yawalkar, A. A., Pangarkar, V. G., Baron, G. V. (2001). Alkene epoxidation with peroxide in a catalytic membrane reactor: a theoretical study. *J. Membr. Sci*, 182, 129.
[95] Nagy, E. (2007). Mass transfer through a dense, polymeric, catalytic membrane layer with dispersed catalyst. *Ind. Eng. Chem. Res*, 46, 2295.
[96] Sousa, J. M., Cruz, P., Mendes, A. (2001). Modeling a catalytic polymeric non-porous membrane reactor. *J. Membr. Sci*, 181, 241.
[97] Sousa, J. M., Cruz, P., Mendes, A. (2001). A study on the performance of a dense polymeric catalytic membrane reactor. *Catal. Today*, 67, 281.
[98] Sousa, J. M., Cruz, P., Magalhães, F. D., Mendes, A. (2002). Modeling catalytic membrane reactors using an adaptive wavelet-based collocation method. *J. Membr. Sci*, 208, 57.
[99] Sousa, J. M., Mendes, A. (2003). Modelling a dense polymeric catalytic membrane reactor with plug-flow pattern. *Catal. Today*, 82, 241.
[100] Sousa, J. M., Mendes, A. (2003). Simulation study of a dense polymeric catalytic membrane reactor with plug-flow pattern. *Chem. Eng. J*, 95, 67.
[101] Sousa, J. M., Mendes, A. (2004). Simulating catalytic membrane reactors using orthogonal collocation with spatial coordinates transformation. *J. Membr. Sci*, 243, 283.
[102] Sousa, J. M., Mendes, A. (2005). Modelling a catalytic membrane reactor with plug-flow pattern and a hypothetical equilibrium gas-phase reaction with $\Delta n \neq 0$. *Catal. Today*, 104, 336.
[103] Sousa, J. M., Mendes, A. (2006). Consecutive-parallel reactions in nonisothermal polymeric catalytic membrane reactors. *Ind. Eng. Chem. Res*, 45, 2094.
[104] Zheng, J. M., Sousa, J. M., Mendes, D., Madeira, L. M., Mendes, A. (2006). Theoretical analysis of conversion enhancement in isothermal polymeric catalytic membrane reactors. *Catal. Today*, 118, 228.
[105] Koros, W. J., Ma, Y. H., Shimidzu, T. (1996). Terminology for membranes and membrane processes. *J. Membr. Sci*, 120, 149-159.
[106] Brandão, L., Madeira, L. M., Mendes, A. M. (2007). Mass transport on composite dense PDMS membranes with palladium nanoclusters. *J. Membr. Sci*, 288, 112.
[107] Brandão, L., Fritsch, D., Madeira, L. M., Mendes, A. M. (2004). Kinetics of propylene hydrogenation on nanostructured palladium clusters. *Chem. Eng. J*, 103, 89.
[108] Brandão, L., Fritsch, D., Mendes, A. M., Madeira, L. M. (2007). Propyne hydrogenation kinetics over surfactant-stabilized palladium nanoclusters. *Ind. Eng. Chem. Res*, 46, 377.
[109] Turner, J. R. (1990). *Colnew*. Chemical Engineering Department, Washington University.

[110] Petzold, L. R., Hindmarsh, A. C. (1997). *Lsoda*. Computing and Mathematics Research Division, Lawrence Livermore National Laboratory.